# Turbulence anisotropy in a compound meandering channel with different submergence conditions

Mera, I. [a]; Franca, M. J. [b]; Anta, J. [a]; Peña, E. [a]

[a] *Water and Environmental Engineering Group- University of A Coruña. ETSI Caminos, Canales y Puertos. Campus de Elviña s/n, 15071 A Coruña, SPAIN. Emails: imera@udc.es, jose.anta@udc.es, epena@udc.es*

[b] *Laboratoire de Constructions Hydrauliques (LCH) - École Polytechnique Fédérale de Lausanne. Station 18, LCH-ENAC-EPFL CH-1015 Lausanne, SWITZERLAND. Email: mario.franca@epfl.ch*

**ABSTRACT (100-150 words)**

The understanding of the physical processes related to flows on compound meandering channels is a challenge given their highly 3D and complex characteristics. Three-dimensional ADV measurements were made in three cross-sections on a 1:20 physical Froude model of a real reach in River Mero (A Coruña) for bankfull flow and flood conditions. General characteristics and processes within the flow are herein described and characterized, such as momentum and mass exchange between the main channel and the floodplains. Time-averaged velocities and Reynolds stresses are presented and discussed. The spatial distribution of turbulence in several positions along a meander bend is analyzed in this paper. The characterization of the turbulent field in these highly 3D complex flows highly depends on the used reference system, and the intense local variation of turbulence makes a global and fixed coordinate system of petty use. An independent technique, regardless the coordinate system of the measurements, is thus the best way to analyse these flows. The anisotropy invariants technique was used to analyze the evolution of the magnitude and nature of anisotropy along the meander. The degree and nature of anisotropy was identified, and their relation to flow structures, such as vortices in the contact between the main channel and the floodplains, was analyzed using the quadrant analysis technique.

*Keywords: meanders, compound channels, turbulence anisotropy, physical model, ADV*

## 1. Introduction

River management represents a challenge from an engineering, environmental and social point of view. In particular, floodplains are among the most productive and diverse ecosystems in the world due to the regular deposition of nutrient rich sediments (*Viers et al. 2005*). The environmental value of these ecosystems is unquestionable given their high biodiversity and their role on water purification and on the fixation of soil and nutrients. Furthermore, floodplains can be seen as natural systems providing food availability and flood protection. The capacity to act as a natural protection against floods is conditioned and intrinsically related to the local hydrodynamics, erosion and sedimentation processes and to the global resistance of the river reach. Flow properties, more specifically related to turbulent phenomena, need a good physical understanding so engineers can address such important issues such as flood management, morphology evolution and spreading of pollutants in river flows (*van Balen et al., 2010*). The physical processes underlying the formation of meanders have been the subject of intensive and detailed research (i.e. *da Silva, 2006; de Marchis and Napoli, 2008; Stoesser et al., 2010*), although the theoretical developments taking into account compound meandering channels are still scarce.

Compound meanders usually appear in the final, low reaches of rivers. Their hydrodynamics are commonly characterized by the existence of two flow layers associated to the main channel and the floodplains. The floodplain flow plunges into the main channel along the inner margin of the bend and the water in the main channel is ejected towards the floodplain in the outer part of the curve (*Sellin et al., 1993*). Coherent vortices developed at the boundary between these two regions (*Proust et al., 2013*) enable momentum exchange and induce extra friction of turbulent nature (*Muto, 1997*). Also, vertical vortices appear in the contact between main channel and floodplain (*Sanjou and Nezu, 2009*). Hence, the turbulent pattern is also characterized by a vertically two-layer structure around the main channel-floodplain interface, as stated by *Carling et al. (2002)*. These turbulent processes produce changes in the morphology of the channel bed, such as dunes and bars (*Yalin, 2006*) that modify the flow dynamics. Their magnitude and orientation are directly related to the flow resistance and sediment transport processes.

The flow in compound meandering channels is hence tridimensional, and reorientation occurs along vertical and transverse directions. Some authors have analyzed the hydrodynamics of curved channels (*Blanckaert and de Vriend, 2005*; *Termini and Piraino, 2011, Abad et al., 2013*) and straight compound channels (*Knight and Shiono, 1990*; *Koziol, 2013*). However, the experimental studies focused on compound meandering morphologies are scarce (*Shiono and Muto, 1998*; *Shiono et al., 2008*) and refer to simplified sinusoidal channels. This work analyzes a river reach with real planform and transversal morphology, geometry features that add complexity to the flow.

This paper is focused on a real case of a compound meandering reach in River Mero (A Coruña), where natural bed irregularities and roughness heterogeneity add complexity to the hydrodynamic pattern. Laboratory measurements are performed intensively in key cross-sections of a physical scaled model of this river reach. The studied area is paradigmatic from a compound meandered channel flows and real features were introduced in the scale model. A scale model of a real case, although reduces the generalization of the research results, induces extra complexity which needs to be adequately tackled.

The shear stresses and turbulence patterns are analyzed in detail. The existence of turbulent structures with particular orientations may be related to hydrodynamic patterns, such as the preferred flow direction, the existence of vortices in the shear layer formed between different water masses or the presence of solid or hydrodynamic boundary conditions.

Reference frames based on the channel geometry may be too rigid to analyze flow features with this degree of re-orientation and tridimensionality. Other systems, related for example to the local flow velocity, can vary too much along the model (*Mera, 2014*). To overcome these limitations, the technique of the anisotropy invariants proposed by *Lumley and Newman (1977)* provides a methodology to analyze the turbulence which is irrespective of the reference system. It allows the characterization of its spatial distribution in terms of anisotropy degree and nature. *Smalley et al. (2002)* applied this technique to velocity measured in near-wall turbulent boundary layers with different values of roughness and concluded. The only reported results of the application of this methodology to flow in complex morphologies are the presented by *Van Balen (2011)*, applied to numerical results from simulations of the flow in sharp open-channel bends. Finally, the quadrant analysis technique is used here in order to link the anisotropy results to the existing hydrodynamic pattern.

The objective of this paper is to characterize the hydrodynamics and the turbulence pattern in a real compound meandering channel. This is accomplished by using the anisotropy invariants and the quadrant analysis techniques. The preliminary application of this methodology to previous results in some specific locations obtained in the same physical model can be found in *Mera et al. (2012)*.

## 2. Theoretical framework

A first description of the flows studied in this paper is made by computing and analysing time-averaged velocities and Reynolds stresses. Standard Reynolds decomposition, followed by application of time-averaged operators, implies the appearance of Reynolds stresses (extra sinks) in the momentum conservation equations which are later shown and commented in this document.

By far less common on the analysis of fluvial flows is the use of the so-called Lumley triangle technique, which is thus hereinafter described in detail. This technique, proposed by *Lumley and Newman (1977),* is based on the analysis of the anisotropy tensor $b_{ij}$, which is the result of decomposing the Reynolds stress tensor into an isotropic and a non-isotropic term:

$$b_{ij} = \frac{\overline{v_i' v_j'}}{2 \cdot k} - \frac{\delta_{ij}}{3} \quad (1)$$

where $v_i'$ is the instantaneous velocity fluctuation in the direction *i*, $\delta_{ij}$ is Kronecker´s delta function and $k$ is the turbulent kinetic energy of the flow defined as

$$k = \frac{1}{2}\left(\overline{v'^2_1} + \overline{v'^2_2} + \overline{v'^2_3}\right) \quad (2)$$

Lumley´s theory is based on the analysis of the anisotropy tensor´s invariants. $b_{ij}$ has two non-null independent invariants, which are (*Lumley and Newman, 1977)*

$$II = -b_{ij} b_{ji} \quad (3)$$

$$III = b_{ik} b_{kj} b_{ji} \quad (4)$$

Plotting *III* against *-II*, the domain of both invariants is reduced to the interior of a curved triangle, as shown in Figure 1. The limits of this triangle define several characteristic states of the turbulence. The origin of the graph (*-II = 0*, *III = 0*) corresponds to 3D isotropic turbulence, where the three normal stresses are equal. The transition from 3D to 2D and/or to 1D turbulence is delimitated by two characteristic types of turbulent structures: pancake-shaped turbulence corresponding to a situation where two of the fluctuation components are equally distributed and with considerably higher amplitude than the third; and cigar-shaped structures where two of the turbulence components, and hence normal stresses values, are similar with the third component substantially higher. These two types of structures of turbulence can be interpreted as transition states, the former from 3D to 2D turbulence – if the lowest component vanishes – and the latter from 3D to 1D turbulence – if the cigar-shaped structure is extremely stirred and becomes a line. The upper boundary and vertex correspond to isotropic 2D and 1D turbulence, respectively, and the areas far and within from the mentioned limits represent general tridimensional turbulent conditions. Any turbulence state must be within the limits of the Lumley plots, and it can be said that *–II* represents the degree of anisotropy, while *III* indicates its nature. Another variable evaluating the flow anisotropy is the parameter *J=1-9(0.5II-III)* proposed by *Jovanović (2004)*, which indicates a two-component turbulence when it is close to zero and isotropic turbulence if *J*=1.

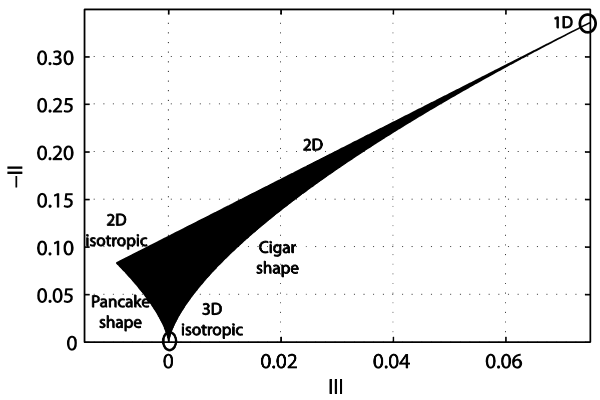


FIGURE 1. Lumley-triangle, adapted from *Lumley & Newman (1977).*

## 3. Materials and methods

This work makes use of a physical scale model of a real meander in river Mero (Cambre, NW of Spain, see location and details in Figure 2). The reach herein analyzed consists of two consecutive low-radius bends contained by protection embankments in both margins. Main channel width ranges from 12 to 14 m, while its mean depth is approximately 2.5 m and its longitudinal slope is 0.0015. Floodplains of the river reach under analysis are commonly flooded to when a compound meandered flow happens. The roughness of the reach is defined by two characteristic areas, corresponding to the main channel and the vegetated floodplains.

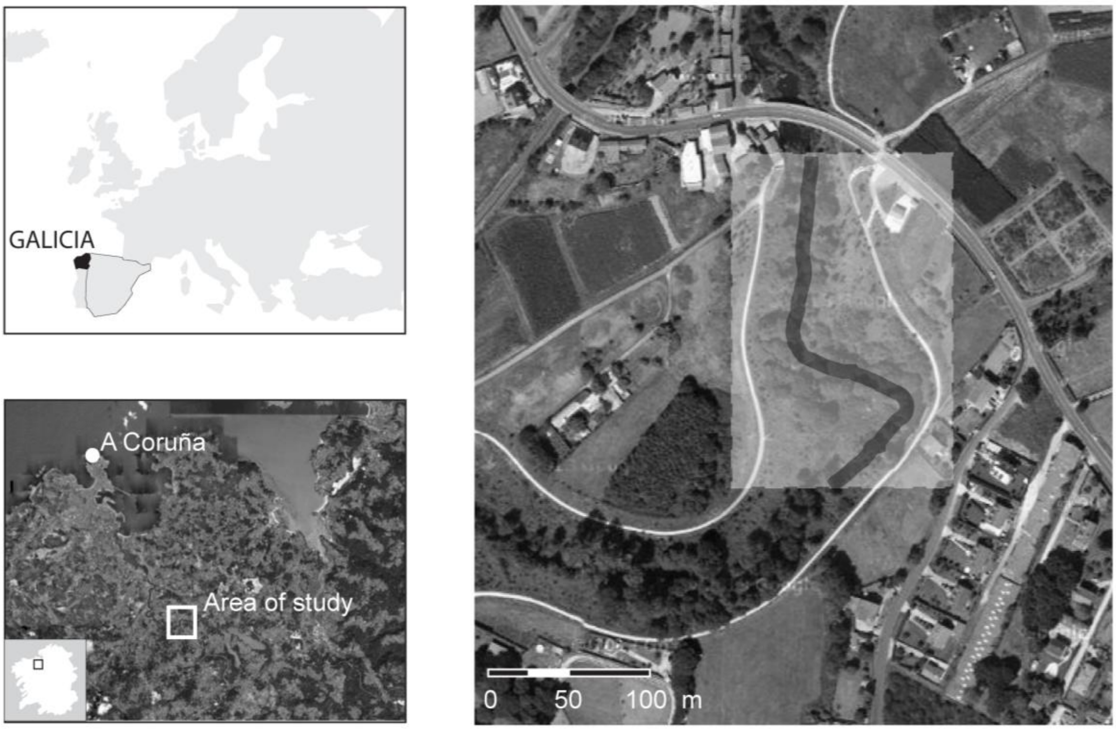


FIGURE 2. Localization of the compound meander of river Mero under study.

The results presented in this work are based in the measurements carried out in a physical model of the described meander (Figure 3). The model was built in the Center for Technologic Innovation in Building and Civil Engineering (CITEEC) of University of A Coruña (Spain). A detailed topographic study of the area, including the main channel and the floodplain, was made in order to reproduce accurately in the laboratory the morphology of the meander. Geometric scale was defined according to the limitation on the laboratory space, resulting in a factor of $\lambda_L$=20. Prototype flow characteristics have been simulated in the model following Froude similarity. Also, both main channel and floodplain roughness in the model are the result of scaling the values of Manning coefficient ($n$) estimated for the real river reach. The resulting values of $n$ for the floodplains and the main channel are $n_{fp}$=0.023 and $n_{mc}$=0.015, respectively. The inlet section of the model simulates an existing bridge, and a unique tank was used for the water supply. As for the downstream boundary condition, the flow was partially obstructed with plastic panels, imposing uniform regime in the reach.

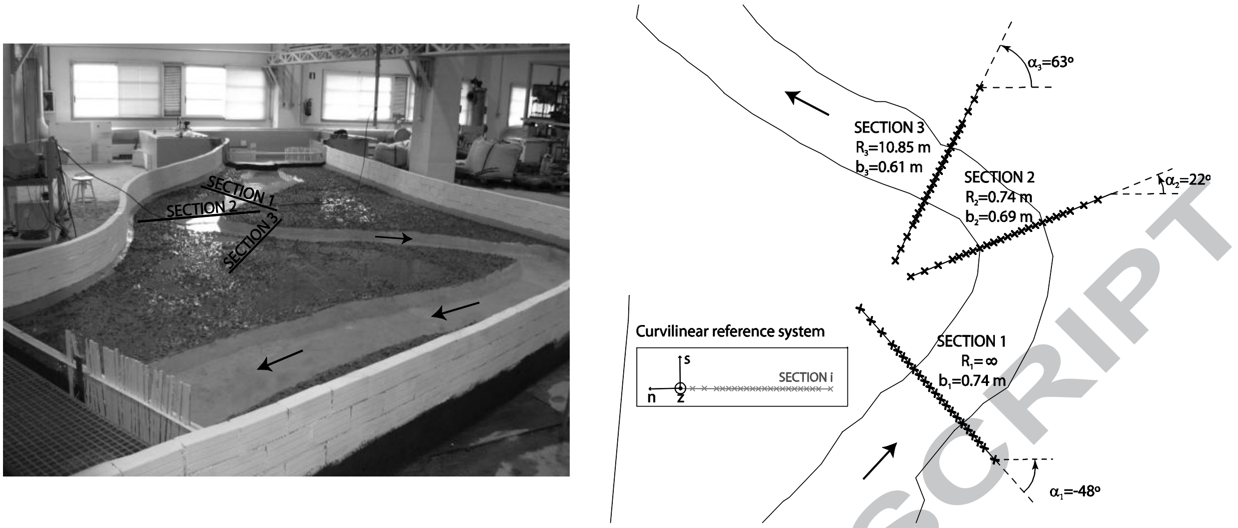


FIGURE 3. Physical model, measurement grid and curvilinear coordinate system. R: curvature radius, b: main channel width.

Initially, water depth and tridimensional velocities were measured for three flow scenarios, including bankfull flow and flooding conditions. This work analyzes the results referred to Experiments 2 and 3, where water flows both, along the main channel and the floodplains. Three transverse sections, carefully chosen to capture important 3D complex features of the flows, were defined to study the flow before, during and after the first bend of the meander (see Figure 3). Section 1 is located in the initial straight reach of the model, Section 2 at the first bend apex, approximately 60° after its beginning, and Section 3 in the crossover region, which is the straight transition zone between the bends, where the main channel and the floodplain direction are roughly orthogonal (see Figure 3). All the results are referred to a curvilinear reference system established for each section. It is defined by the main channel streamwise and transverse directions (*s* and *n*, respectively) and a vertical axis *z*, in the opposite direction of the gravity acceleration.

Table 1 summarizes the hydraulic characteristics of each experiment. The hydraulic bulk parameters of each experiment were calculated based on Section 1, because it is the unique for which a clear transverse direction can be defined across the main channel and the floodplain. Shear velocity was estimated using Darcy´s friction coefficient $f$ ($u^*=(f \cdot U_s^2/8)^{1/2}$ and $f=n_{eq}^2 \cdot 8 \cdot g/R_h^{1/3}$). An equivalent composite roughness value of Manning coefficient ($n_{eq}$) was calculated using the well-known Horton-Einsten method. Mean velocity was set as $U_s=Q/A$, and the water depths were measured using ultrasonic probes. As for *Re* and *Fr*, they were calculated using the mean velocity $U_s$ and an equivalent water depth $h_e$. The latter is a weighting of main channel and floodplains water depths, according to their cross-sectional area.

TABLE 1. Experimental tests characteristics: discharge (*Q*), mean velocity ($U_s$), shear velocity ($u^*$), mean water depth in the main channel ($h_c$) and the floodplain ($h_f$), relative depth ($D_r$), Reynolds ($Re=U_s \cdot h_e/v$) and Froude ($Fr=U_s/(g \cdot h_e)^{1/2}$) numbers

| | Discharge L/s | Mean velocity m/s | Shear velocity m/s | Channel flow depth m | Floodplain flow depth m | Relative depth | Re | Fr |
|---|---|---|---|---|---|---|---|---|
| Experiment 2 | 35 | 0.093 | 0.010 | 0.190 | 0.050 | 0.26 | 8649 | 0.097 |
| Experiment 3 | 60 | 0.099 | 0.010 | 0.235 | 0.090 | 0.38 | 12177 | 0.090 |

Detailed vertical instantaneous velocity profiles have been measured for several positions along these sections. 3D instantaneous velocities were measured using a four-receiver ADV equipment (Vectrino form Nortek®), during 300 s at a 25 Hz acquisition frequency. The total record time proved to be enough to have stable second order moments of the measured velocities. Data were filtered using phase-space methodology proposed by *Goring and Nikora (2002)* and spatially smoothed across each transverse section with a median filter based on the method proposed by *Westerweel and Scarano (2005)*.

The lowest measuring position is located 2 cm above the model bed and the vertical distance between gates is 2 cm, with a higher resolution (0.5-1 cm) in the contact between the main channel and the floodplain. Following the example of *Franca et al. (2008),* a 8 cm diameter plastic housing with a mylar window on the bottom was constructed to accommodate the ADV probe, allowing thus to register velocities in the upper region of the flow, almost until the free surface.

## 4. Results and discussion

### *4.1. General description of the flow*

Flows in compound meandering channels with overbank water circulation can be described as a two layer flow: a lower region from the bottom to the maximum height of the main channel, and an upper layer covering the water column from the latter depth until the surface (*Shiono and Muto, 1998*). Figure 4 presents the average horizontal velocity vectors in these two layers of the physical model for *Q*=35 and *Q*=60 L/s. The averaged height of the main channel, used for the computation of each layer velocity, is 0.12 m.

A reduction of the mean velocity in the central part of the model (around the transition zone between the two bends) is observed for both cases, caused by the increasing floodplain width. For the low submergence flood (Q=35 L/s), the lower region of the flow clearly follows the direction of the main channel in Sections 1 and 3, similarly to a bankfull situation (*Mera, 2014*), while the direction of the flow in the upper layer follows the floodplain direction. A realignment of the water circulation in the channel lower layer is observed in the bend apex (Section 2) and disappears once the crossover region is reached (Section 3). This is coherent with the results of *Shiono and Muto*

*(1998)* and the theory of generation, saturation and disappearing of secondary currents (*Blanckaert, 2009; Van Balen, 2011*).

The magnitude of the horizontal velocity decreases in the inferior layer for $Q$=60 L/s. The variation of the flow direction along the bend is also observed in this scenario. However, the influence of the floodplain is fairly more significant, to the point that the flow follows its direction even in the lower layer of Section 3. Negative streamwise velocities appear in this area, caused by the plunging and recirculation of the upper flow in the main channel, as pointed by Sellin *et al.* (1993) for the crossover region. The analysis of three velocity components in all the measurement positions -not shown here, see *Mera (2014)* for further illustration of this– reflects flow tridimensionality, in particular in the contact surfaces between the main channel and the floodplain, and shows also that momentum exchange occurs in these areas.

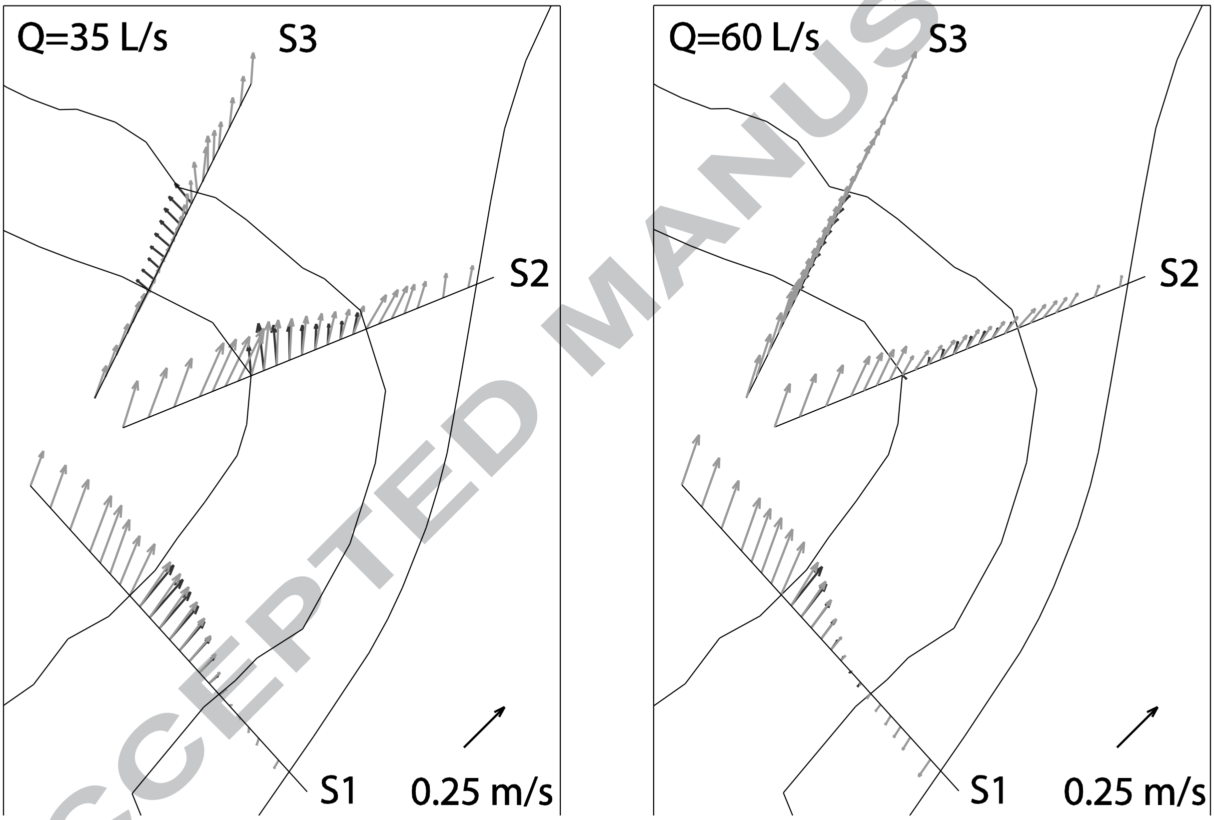


FIGURE 4. Average horizontal velocity in the lower (black) and upper (grey) layers of the flow in the first bend of the meander for $Q$=35 and $Q$=60 L/s.

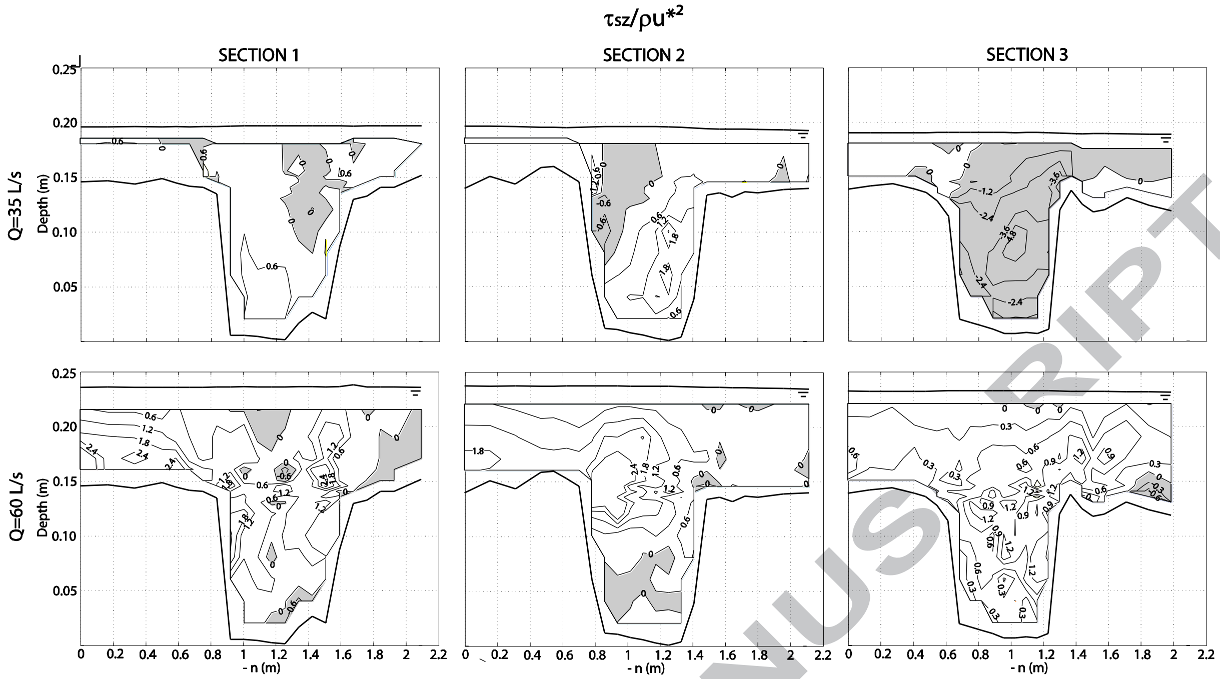


FIGURE 5. Dimensionless value of $\tau_{sz}$ for Q=35 and Q=60 L/s. Areas of negative values are shaded.

In Section 3, water in the floodplains flows along the spanwise direction for both flood conditions. Hence, flow perpendicular to the main channel direction has a great importance and promotes the income of water from the floodplain to the main channel, enhancing flow tridimensionality. The friction between the upper and bottom layer generates shear stress in this interface. Figure 5 shows the value of the shear stress in the longitudinal-vertical plane $\tau_{sz}$ normalized by $\rho u_*^2$ in Sections 1, 2 and 3 for the two flood scenarios. Positive values are associated to the entrance of water from the floodplain to the main channel, while negative ones point the reverse process (*Shiono and Muto, 1998*). Results for *Q*=35 L/s are coherent with this rule: $\tau_{sz}$ is positive in almost the entire Section 1. The positive core below the main channel height in Section 2 indicates that the streamwise velocity in the near-surface layer is higher than in the lower one, and hence the momentum is transferred towards the bottom. This core disappears after the bend, where generally negative values are observed, caused by the ejection of water from the main channel towards the floodplain along the right part of Section 3.

This phenomenon is not observed for Q=60 L/s. The drag exerted by the floodplain flow on the main channel reduces the vertical reorientation of the flow, and the longitudinal velocity gradient is mainly positive along the vertical. This justifies the positive sign of $\tau_{sz}$ in the three sections. Small negative areas are observed in the right margin of Section 1 and the bottom of Section 2. Both of them are counterflow areas (see Figure 4): the former is related to the existence of a vertical vortex due to the entrance of the water in the model, and the latter is caused by the plunging of water from the floodplain in the bottom of the main channel.

The generation of a horizontal shear layer is observed in the two flood scenarios. However, low values of $\tau_{sz}$ are observed in areas of expected friction, such as the main channel and floodplain contact of Section 2. The analysis of shear stress in the horizontal plane $\tau_{sn}$ (Figure 6) shows significant values of this component in areas of relevant transverse circulation. In these surfaces, the friction between the two flow layers may occur along the spanwise direction *n*. This confirms the substantial turbulence anisotropy commented by *Carling et al. (2002)*: $\tau_{sz}$ is predominant near the channel bed and $\tau_{sn}$ around the free surface.

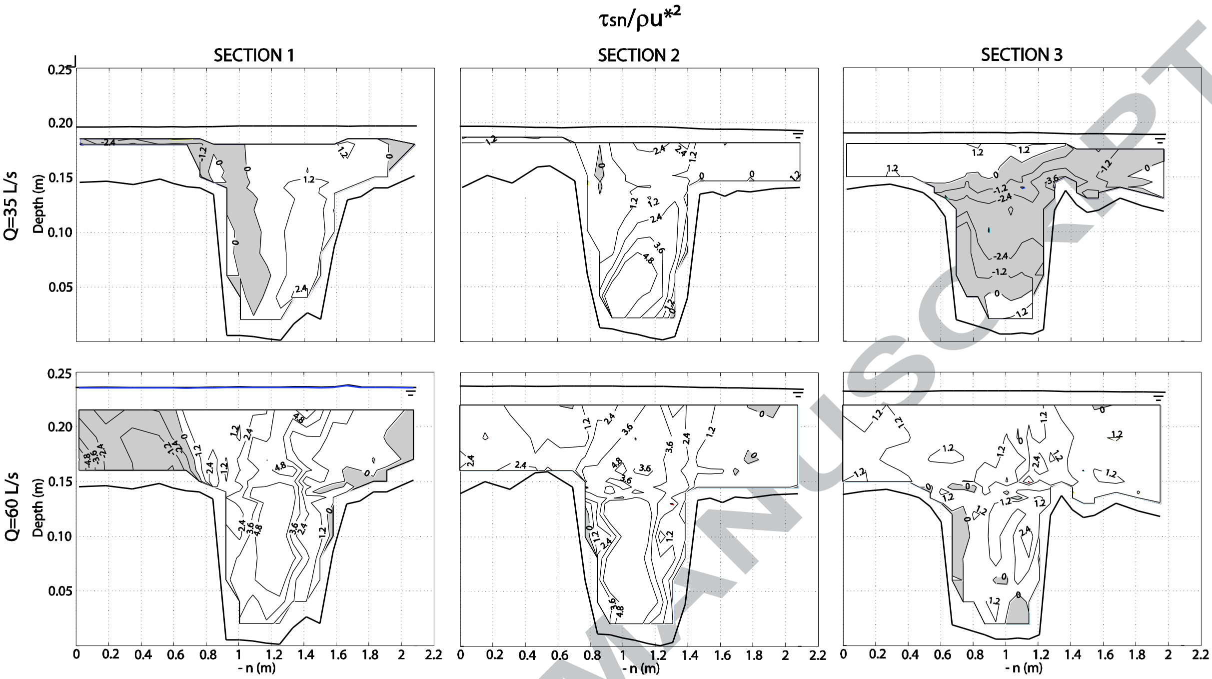


FIGURE 6. Dimensionless value of $\tau_{sn}$ for Q=35 and Q=60 L/s. Areas of negative values are shaded.

Shear stress patterns are affected by the channel morphology: the existence of bends and/or floodplains determines the hydrodynamic regime flow (*Mera et al., 2011*). Hence, in compound meanders, turbulence cannot be evaluated through a unique component of the stress tensor. A technique that analyses the turbulence from a global point of view may be of help to characterize the shear in flows of this kind. The anisotropy invariants technique, as introduced by *Lumley and Newman (1977)*, is applied to these results in the next section of this paper as an alternative to the more traditional analysis based on Cartesian coordinates.

*4.2. Analysis of turbulence anisotropy*

*4.2.1. General description of the anisotropy pattern*

Figure 7 shows the transverse maps of the parameter *J* (as defined by *Jovanović, 2004*) for the analyzed sections and flow scenarios. These results provide a first insight in the anisotropic pattern of the turbulence in the physical model. There is a general trend to the isotropic turbulence, since *J*>0.5 throughout the sections. In all the cases the areas with lowest values of *J* appear near the model walls and water surface, because in these areas the components orthogonal to the boundary condition tend to zero. Maximum values of *J* are concentrated in the main channel-floodplain contact at sections 1 and 2, which may be related to the high level of water exchange in those areas. In Section 3 the values of *J* are segregated by depth: high values are found in the main channel area near the bottom, and they decrease in the upper part of the flow. This indicates a vertical evolution of the turbulence, from a more isotropic state in the bottom towards a two-dimensional one in the floodplains.

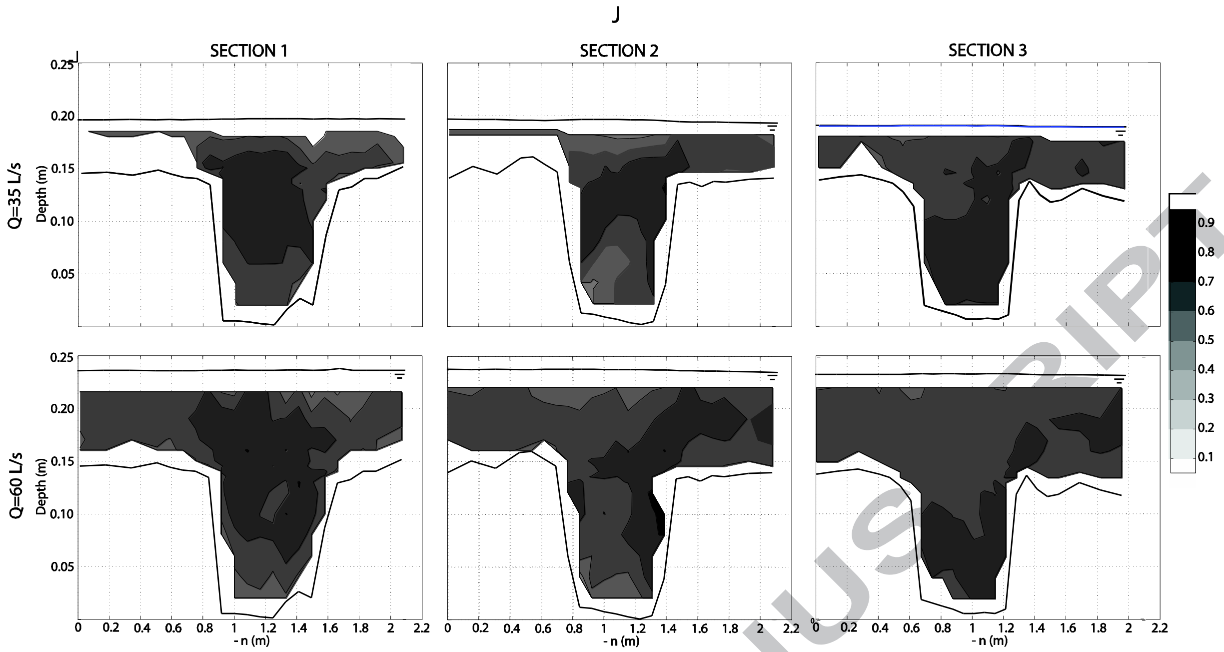


FIGURE 7. Distribution of the parameter $J$ (*Jovanović, 2004*) for Q=35 and Q=60 L/s. $J$=0 (white) indicates two-component turbulence and $J$=1 (black) an isotropic state.

*4.2.2. Vertical distribution of the anisotropy invariants*

As mentioned in the Section 2 of this paper, the application of the so-called Lumley´s triangle technique quantifies the degree and nature of the turbulence anisotropy in a certain flow. In this section, the evolution of the invariants $-II$ and $III$ across the $z$ direction is analysed in order to search a relation between the spatial distribution of the turbulence and the vertical position. Three areas have been defined to characterize the flow: the main channel ($z \leq 0.10$ m), the floodplains ($z \geq 0.15$ m); and the area of interaction between these two regions (0.10 m < $z$ < 0.15 m). The average depth of the main channel is 0.12 m. Figure 8 shows the anisotropy invariants in all the measurement positions for the Experiments 2 and 3 grouped by the criterion of position.

In the low submergence test a trend to cigar-shaped turbulence is observed in the low and intermediate layers of the flow in Sections 1 and 2 for Q=35 L/s, whereas general tridimensional and pancake structures characterize the water circulation near the surface. In Section 3 the behaviour of the three flow layers is similar and the results are mostly far from the cigar-shape limit. However, some differences between them can still be observed, such as the increasing level of anisotropy from bottom towards the surface.

In the high submergence scenario, the vertical evolution of the turbulence anisotropy is less clear. Some points of the surface zone approach to the cigar-shape limit in Section 1, while others belonging to the interaction region appear far from it in Section 2. Again, the results are gathered between the 2D and the cigar anisotropy limits, far from both of them, in Section 3. The points from the intermediate and high layers of the flow fill the same region of the Lumley triangle. This indicates that, in Experiment 3, the dynamics of the interaction region are similar to those of the floodplain flow.

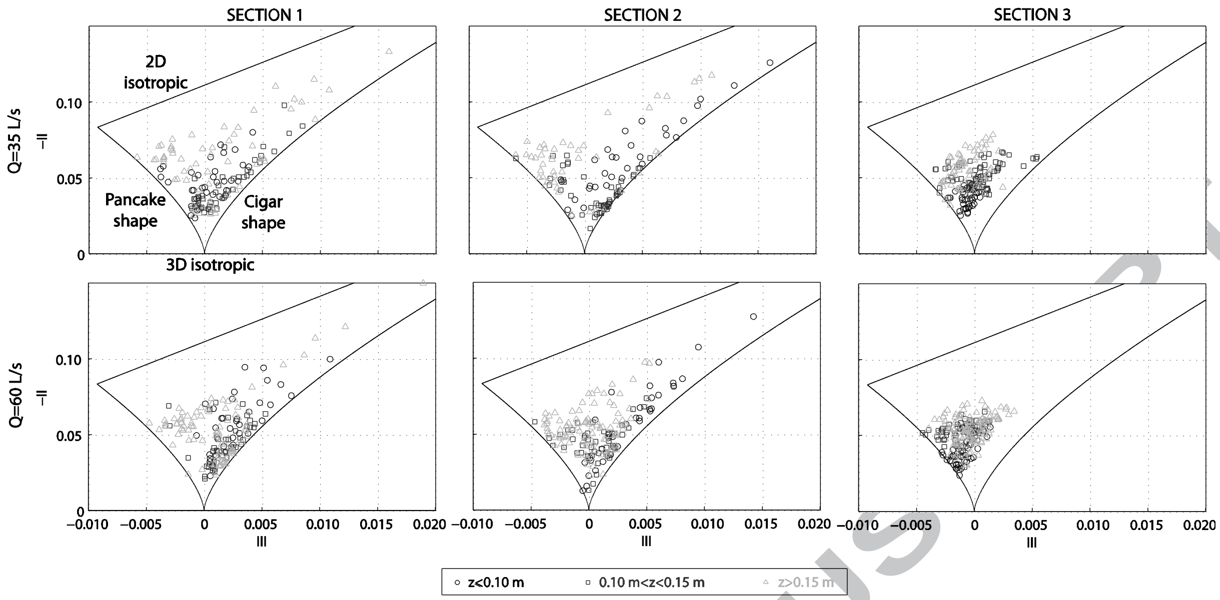


FIGURE 8. Distribution of the anisotropy invariants throughout the water column for the three sections grouped by flow layers.

The vertical evolution of the anisotropy pattern and its relation to the submergence level can be analyzed in detail through the results obtained for a vertical profile in the centre of Section 2 (spanwise coordinate $n \approx 1.1$ m) for the two flooding scenarios (see Figure 9). In the case of low submergence (Q=35 L/s), most of the profile is characterized by cigar type structures, which indicates the existence of a predominant direction of the velocity fluctuation. Only some points near the bottom and the surface present a general tridimensional distribution of the turbulence. For Q=60 L/s the results are shifted to the left in the Lumley triangle, and hence distancing from two-dimensional turbulent structures.

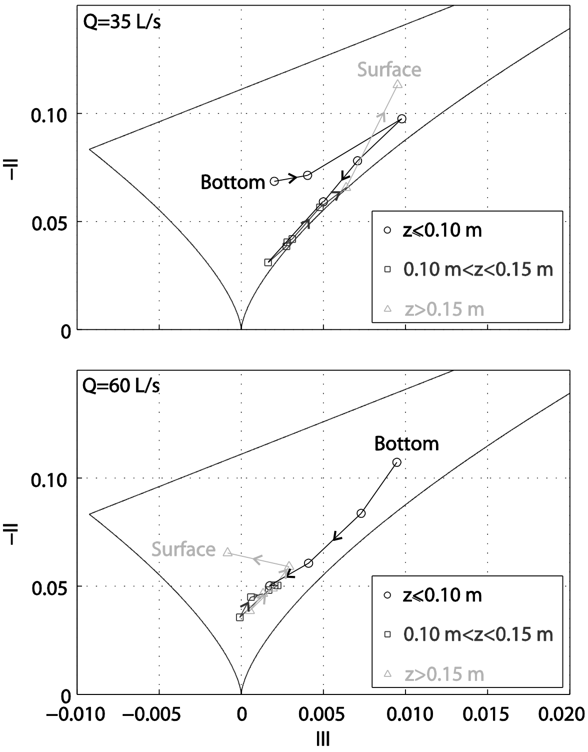


FIGURE 9. Distribution of the anisotropy invariants throughout the water column for two different submergence conditions in the centre of Section 2. The direction from channel bottom to the surface is indicated by the arrowheads.

The evolution of the anisotropy level along the vertical direction may also be of interest in the identification of turbulent structures within the flow. In both profiles the highest degrees of anisotropy (-*II* > 0.05) are observed in the points near the bottom and the water surface, while this value is lower in most of the intermediate region. This points out that, even if the turbulence level in this area is relevant, it doesn´t have a significantly predominant orientation. Actually, according to the results presented in Figure 5, the maximum values of the shear stress in the longitudinal-horizontal plane are observed in the horizontal contact between the main channel and the floodplain.

*4.2.3. Transverse distribution of the anisotropy invariants*

Figure 10 shows the anisotropy invariants divided by the two lateral floodplains and the central main channel, for the three sections. For Q=35 L/s the distribution of turbulence in Sections 1 and 2 varies from the floodplains, where some points are close to the pancake limit, to the main channel, which shows a trend to the cigar-shape boundary and high anisotropy levels in some points. In Section 3 the results are more concentrated, although the turbulence distribution in the main channel still shows a tendency to a unidimensional structure, like the cigar-shaped.

The patterns of turbulence distribution corresponding to Q=60 L/s are similar, section by section, to those of the low submergence scenario.  Similarly to the observed in the vertical direction, in Section 3 is not possible to establish a relation between the transverse position and the distribution of the turbulence. Again, the high level of tridimensionality in these conditions inhibits the predominance of a unique direction of fluctuation.

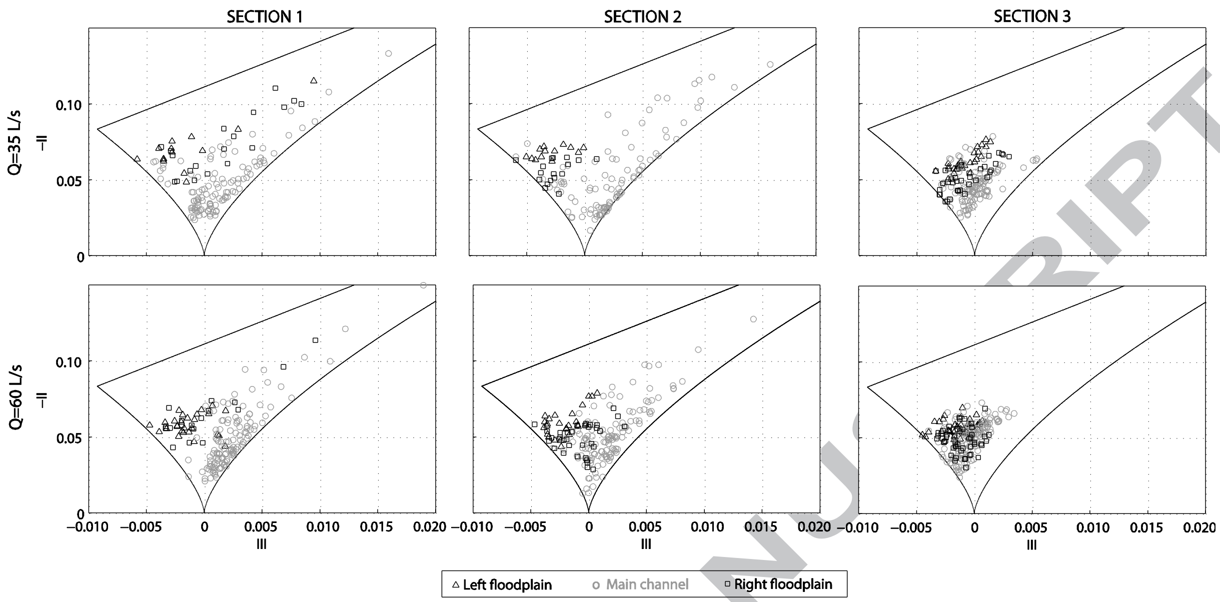


FIGURE 10. Distribution of the anisotropy invariants across the transverse sections.

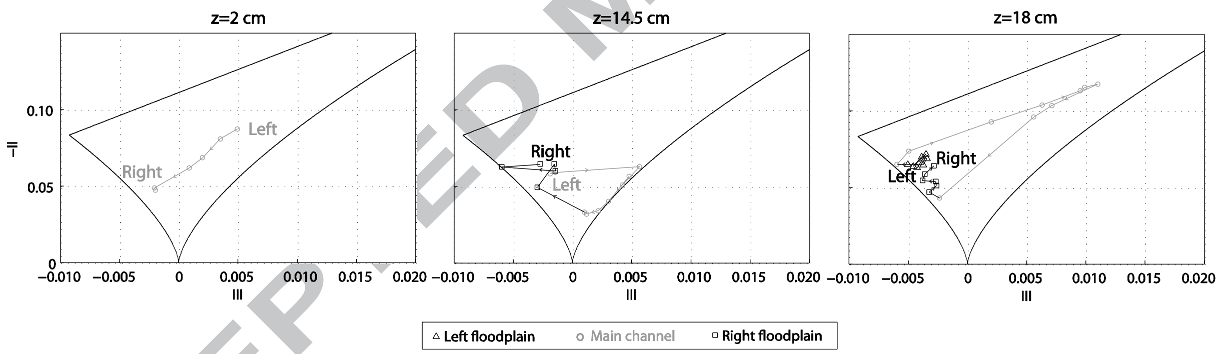


FIGURE 11. Distribution of the anisotropy invariants across the transverse sections for three different depths of Section 2 and *Q*=35 L/s. The direction from the left to the right floodplain is indicated by the arrowheads.

The transverse evolution of the anisotropy invariants at different depths (near-bottom, interaction and near-surface zones) in Section 2 for Q=35 L/s is presented in Figure 11. The turbulence goes from a bidimensional pattern towards a general tridimensional state close to the channel bottom (z=0.020 m). As depth increases, different trends can be observed in the floodplains and the main channel. Along the horizontal interface between both (z=0.145 m) the turbulence evolves from cigar-shaped in the main channel to near-pancake structures in the right floodplain (note that velocities in the left floodplain could not be measured at this depth). The dominant direction of the fluctuation in the main channel structure may be defined by the income of water from the floodplain.

Near the surface (*z*=0.180 m) different trends are also observed, but in this case the turbulence in the main channel shows a high level of anisotropy and does not approach to any particular spatial distribution. In these points the flow is not anymore constrained by the interaction between the main channel and the floodplain, and it is distributed irrespectively of the existence of a lower flow layer. In the same transverse profiles for Q=60 L/s (not presented here) the structure of turbulence in the main channel near the water surface, and even at z=0.145 m, is more similar to that of the floodplains. This indicates that the flow is governed by the floodplain or, which is equivalent, that the influence of the the main channel in the flow is not significant. Hence, the existence of a central meander can be seen such as a large macro-roughness for a flow bounded and guided by the floodplain limits, with little importance on mass and momentum transport. Furthermore, processes related to sediment movement and mass transfer are more important in the main channel for lower flooding conditions.

*4.2.3. Orientation of turbulent structures*

The objective of this section is to relate the spatial distribution of the turbulence to the hydrodynamic structures within the flow. The quadrant analysis technique, usually employed to characterize shear events, has been applied to the results of this work in order to analyze the orientation of some particular anisotropic structures detected with the Lumley triangle. It consists on representing the scatter of the velocity fluctuation components, two by two.

Two positions have been selected for the application of the quadrant analysis technique, both of them in Section 2 for a discharge of Q=35 L/s (see Figure 12). Point P is located above the left wall of the main channel (z=180 mm), and appears on the pancake line in the Lumley triangle. Point C, in centre of the channel at a depth z=150 mm, shows a characteristic cigar distribution.

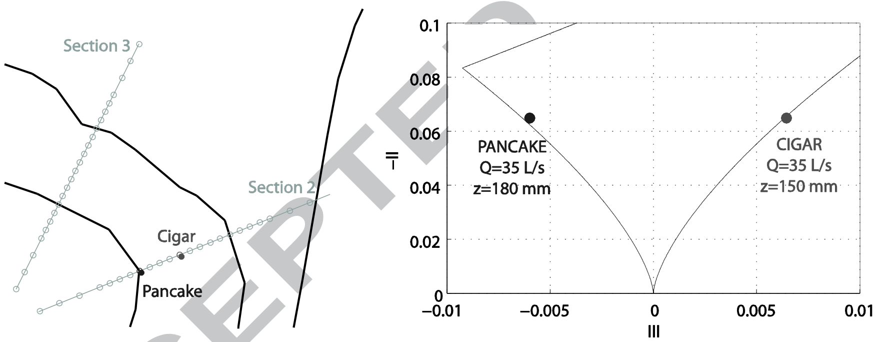


FIGURE 12. Points P and C selected for the quadrant analysis of the turbulent structures orientation.

Coordinate axis referred to the mean horizontal flow at each position *($v_h$*: direction of the horizontal velocity*, $v_p$*: horizontal direction orthogonal to *$v_p$,z*) have been used to represent the quadrant analysis and identify the orientation of the selected turbulent structures. Figure 13 shows the results referred to pancake point P according to this *($v_h$,$v_p$,z)* coordinate system. The value of the 95th percentile is specified for each direction ( $v'i_{95}$, $|v'_i| \le v'i_{95}$ for the 95% of values of $v'_i$ ). The results present a dominance of the horizontal components of velocity fluctuation $v'_{vh}$ and $v'_{vp}$, much higher than $v'_z$. This is coherent with the existence of vertical vortices that transfer water from the floodplain to the main channel (*Sanjou and Nezu, 2009*).

Figure 14 shows the results of the quadrant analysis for the cigar point C. In this case, the most relevant fluctuations occur in the direction of $v_p$, which is approximately parallel to the direction of the water entrance from the floodplain to the main channel.

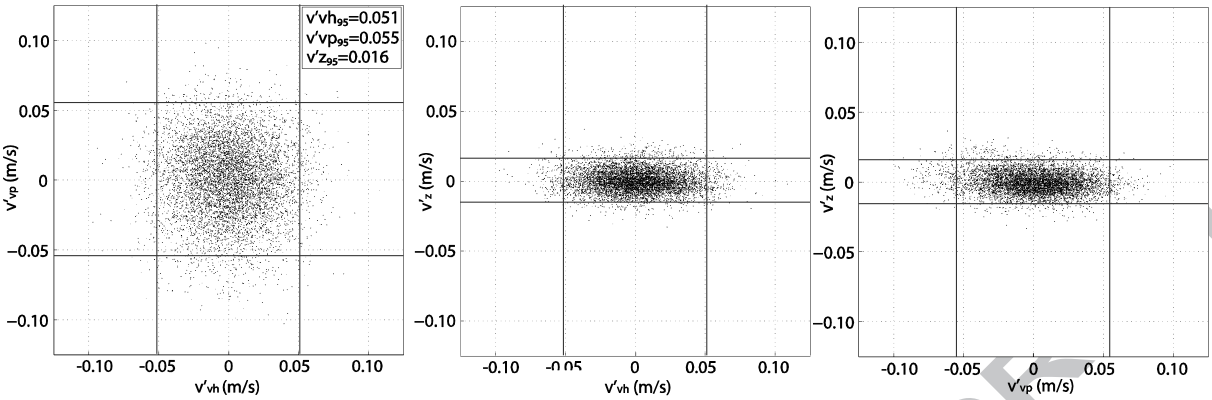


FIGURE 13. Quadrant analysis according to horizontal flow reference system *($v_h$, $v_p$, z)* at position P (pancake-shaped turbulence) for Q=35 L/s.

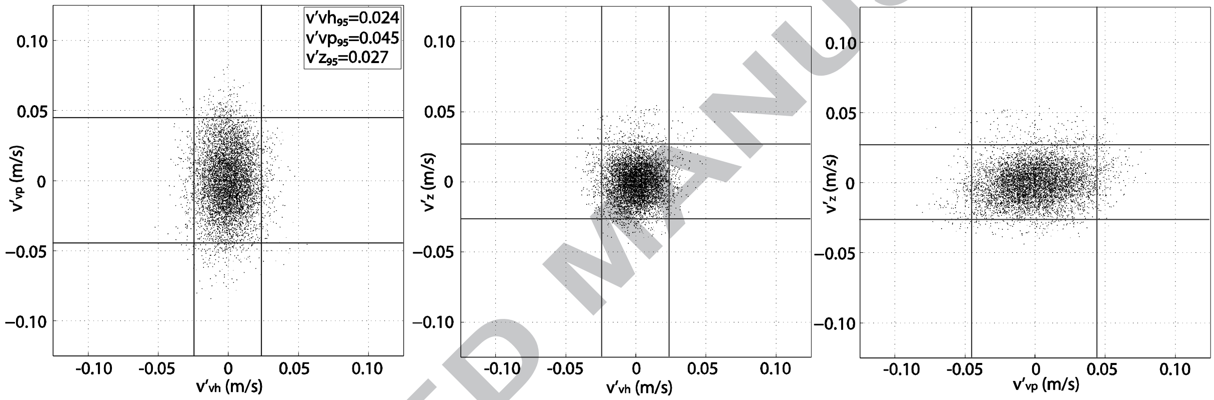


FIGURE 14. Quadrant analysis according to horizontal flow reference system *($v_h$, $v_p$, z)*at position C (cigar-shaped turbulence) for Q=35 L/s.

## 5. Conclusions

The hydrodynamics and turbulent field along a bend of a real compound meandering channel were analyzed using tridimensional velocity measurements performed on a physical scale model. Results of 3D instantaneous velocity measurements made on three cross sections, carefully chosen to represent important features of the flows, were analyzed in this study where a highly tridimensional complex flow is observed. Two different flow relative submergences were studied, corresponding to two different flooding situations.

Water exchange between the floodplains and the main channel generates secondary flow with transversal velocity components in the main channel. The reorientation of the flow along both vertical and transverse directions was observed for the different submergence cases and was more relevant as the divergence between the main channel and the floodplain increased. The low submergence scenario showed a combined contribution of the main channel (lower layer of the flow) and the floodplain (upper layer) to the mass and momentum transport in the compound channel. For the high submergence ratio, the water circulation in the floodplains dominated total flow conveyance, while the main channel acted as macro-roughness that only influenced the flow near the channel bottom. The varying width of the floodplains causes a deceleration of the water flow in the transition between the two bends. This phenomenon was not observed in previous studies referred to constant width models. The analysis of the shear stress distribution showed the occurrence of momentum transfer between the main channel and the floodplain (on both directions), and the generation of a shear layer in the horizontal contact between them. These processes may be relevant to processes of erosion of the channel walls, and hence to morphological changes of the river sections.

The anisotropy invariants technique proposed by *Lumley and Newman (1977)* was applied for the characterization of the turbulent structures of the flow, as an alternative to conventional Cartesian analysis. Different spatial distributions of the turbulence along the vertical direction were observed for the low submergence scenario, from the so-called cigar trend in the lower part of the flow towards a general 3D distribution near the surface. In the high submergence case, the patterns of the intermediate area and the floodplain tend to collapse. Section 3 presented in both cases the most homogeneous pattern. The high degree of tridimensionality in this area, due to the water income from the floodplain to the main channel, limits the development of turbulent structures with a main predominant direction. The distribution of the turbulence showed relevant changes along the transverse direction. Positions in the floodplains (left and right margins) present a tendency to the pancake-shaped turbulence, while those in the centre of the section approach to cigar-shaped limit. These differences are smoothed for the high submergence flood.

The application of the anisotropy invariants technique allowed the identification of flow turbulent features, intrinsically related to the water exchange between the main channel and the floodplain and the vertical vortices in the surface contact between them. Anisotropy degree decreases in areas with a highly tridimensional flow, such as the contact between the main channel and the floodplain, and increases for flood conditions in the upper part of the flow, where the influence of the circulation in the main channel is not significant and general bidimensional flow can be developed.

Finally, some particular turbulent structures were linked to the general hydrodynamic features by means of quadrant analysis technique. The vertical vortices occurring in the contact between the main channel and the floodplain causes horizontal, plane turbulent structures (known as *pancakes*). Water fluxes from the floodplains to the main channel originates turbulent features aligned with the direction of the upper flow.

The results here in presented show that the combination of the anisotropy invariants and the quadrant analysis techniques allows the characterization of turbulence, and the identification of characteristic structures and their orientation. In river flows, where high Reynolds are commonly present, the main source of diffusion of diluted or undiluted species is the turbulent motion. The knowledge of the orientation of the main turbulence states, which can be obtained through the combination of techniques herein presented, allows inferring if there are preferential directions in the flow along which the turbulent transport is more effective.

**Acknowledgements**

The authors thank the economical support of the Spanish Ministry of Science and Innovation, reference project CGL2008-03319/BTE (National Plan of R+D 2008-2011) and the comments and suggestions of the reviewers assigned to this paper. The work herein presented was partially developed during a research stay of Inés Mera at the Faculty of Science and Technology of New

University of Lisbon, under the supervision of Mário J.Franca, whose support the first author would like to thank.

**References**

Abad, J.D., Frias, C.E., Buscaglia, G.C., Garcia, M.H., 2013. Modulation of the flow structure by progressive bedforms in the Kinoshita meandering channel. Earth Surface Processes and Landforms 38 (13), 1612-1622.

Blanckaert, K., 2009. Saturation of curvature-induced secondary flow, energy losses and turbulence in sharp open-channel bends: Laboratory experiments, analysis and modelling. Journal of Geophysical Research B: Solid Earth 114 (3).

Blanckaert, K., de Vriend, H.J., 2005. Turbulence structure in sharp open-channel bends. Journal of Fluid Mechanics 536, 27-48. doi: 10.1017/S0022112005004787.

Carling, P.A., Cao, Z., Holland, M.J., Ervine, D.A., Babaeyan-Koopaei, K., 2002. Turbulent flow across a natural compound channel. Water Resources Research 38 (12), 1270. doi: 10.1029/2001WR000902.

Choi K.-S., Lumley, J.L. 2001. The return to isotropy of homogenous turbulence. Journal of Fluid Mechanics 436, 59-84.

da Silva, A.M.F, 2006. On why and how do rivers meander. Journal of Hydraulic Research 44 (5), 579-590.

De Marchis, M., Napoli, E., 2008. The effect of geometrical parameters on the discharge capacity of meandering compound channels. Advances in water resources 31 (12), 1662-1673.

Franca, M.J., Ferreira, R.M.L., Lemmin, U., 2008. Parameterization of the logarithmic layer of double-averaged streamwise velocity profiles in gravel-bed river flows. Advances in Water Resources 31 (6), 915-925.

Goring, D.G., Nikora, V.I., 2002. Despiking acoustic doppler velocimeter data. Journal of Hydraulic Engineering 128, 117-126. doi: 10.1061/(ASCE)0733-9429(2002)128:1(117).

Jovanović, J., 2004. The statistical dynamics of turbulence. Springer.

Knight, D.W., Shiono, K., 1990. Turbulence measurements in a shear layer region of a compound channel. Journal of Hydraulic Research 28 (2), 175-196.

Koziol, A.P., 2013. Three-dimensional turbulence intensity in a compound channel. Journal of Hydraulic Engineering 139 (8), 852-864.

Lumley, J.L., Newman, G.R., 1977. The return to isotropy of homogeneous turbulence. Journal of Fluid Mechanics 82 (1), 161-178.

Mera, I., 2014. Experimental study of a meander of River Mero (A Coruña). Hydrodynamic characterization of main channel and floodplains for several flooding conditions. PhD Dissertation. University of A Coruña.

Mera, I., Franca, M.J., Anta, J., Peña, E., 2012. Turbulence anisotropy in a compound meandering channel. Proceedings of the International Conference on Fluvial Hydraulics River Flow 2012 *(*1), 79-84. ISBN: 978-146657551-6.

Mera, I., Franca, M.J., Peña, E., Anta, J., 2011. Análisis acimutal de las direcciones principales de las tensiones tangenciales en un canal compuesto meandriforme. Jornadas de Ingeniería del Agua.

Muto, Y., 1997. Turbulent flow in two-stage meandering channels. PhD Dissertation. University of Bradford.

Proust, S., Fernandes, J.N., Peltier, Y., Leal, J.B. , Riviere, N., Cardoso, A.H., 2013. Turbulent non-uniform flows in straight compound open-channels. Journal of Hydraulic Research 51 (6), 656-667.

Sanjou, M., Nezu, I., 2009. Turbulence structure and coherent motion in meandering compound open-channel flows. Journal of Hydraulic Research 47 (5), 598-610.

Sellin, R.H.J., Ervine, D.A., Willetts, B.B., 1993. Behaviour of meandering two-stage channels. Proceedings - ICE: Water, Maritime & Energy, 101 (2), 99-111.

Shiono, K., Muto, Y., 1998. Complex flow mechanisms in compound meandering channels with overbank flow. Journal of Fluid Mechanics 376, 221-261.

Shiono, K., Spooner, J., Chan, T.L., Rameshwaran, P., Chandler, J.H., 2008. Flow characteristics in meandering channels with non-mobile and mobile beds for overbank flows. Journal of Hydraulic Research 46 (1), 113-132.

Smalley, R., Leonardi, S., Antonia, R., Djenidi, L., Orlandi, P., 2002. Reynolds stress anisotropy of turbulent rough wall layers. Experiments in Fluids 33 (1), 31-37.

Stoesser, T., Ruether, N., Olsen, N.R.B., 2010. Calculation of primary and secondary flow and boundary shear stresses in a meandering channel. Advances in Water Resources 33 (2), 158-170.

Termini, D., Piraino, M., 2011. Experimental analysis of cross-sectional flow motion in a large amplitude meandering bend. Earth Surface Processes and Landforms 36 (2), 244-256. doi: 10.1002/esp.2095.

van Balen, W., 2011. Curved open-channel flows. A numerical study. PhD Dissertation. Delft University of Technology.

van Balen, W., Blankaert, K., Uijttewaal, W.S.J., 2010. Analysis of the role of turbulence in curved open-channel flow at different water depths by means of experiments, LES and RANS. Journal of turbulence 11 (12), 1-34.

Viers, J., Barroux, G., Pinelli, M., Seyler, P., Oliva, P., Dupré, B., Boaventura, G.R., 2005. The influence of the Amazonian floodplain ecosystems on the trace element dynamics of the Amazon River mainstem (Brazil). Science of the total environment 339 (1-3), 219-232.

Westerweel, J., Scarano, F., 2005. Universal outlier detection for PIV data. Experiments in Fluids 39 (6), 1096-1100. doi: 10.1007/s00348-005-0016-6.

Yalin, M.S., 2006. Large-scale turbulence and river morphology. Proceedings of the International Conference on Fluvial Hydraulics River Flow 2006 *(*2), 1243-1249. ISBN: 978-041540815-8.

Figure 1



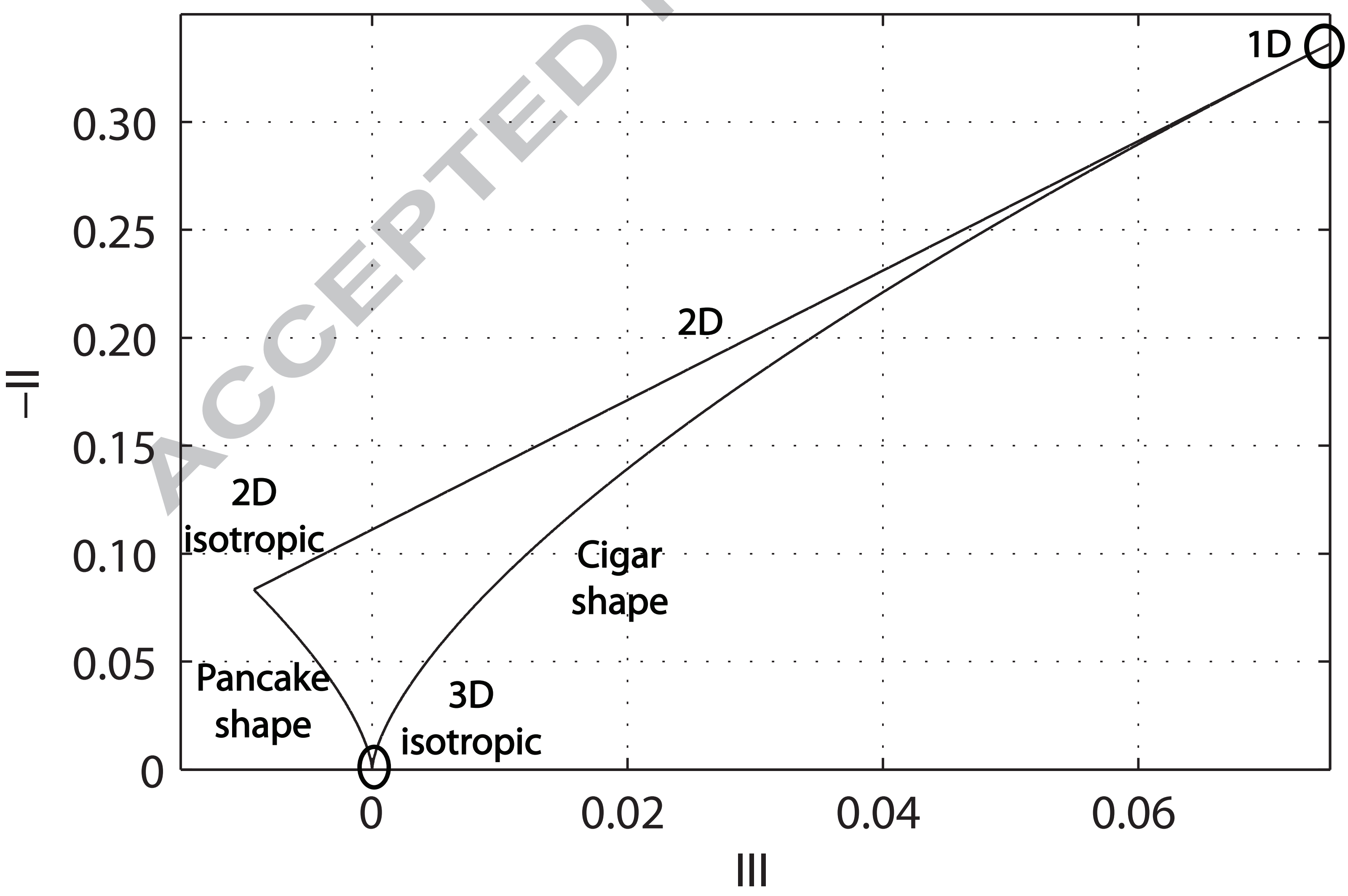

1D
2D
2D
isotropic
Cigar
shape
Pancake
shape
3D
isotropic
0.30
0.25
0.20
0.15
0.10
0.05
0
0
0.02
0.04
0.06
-II
III

Figure 2





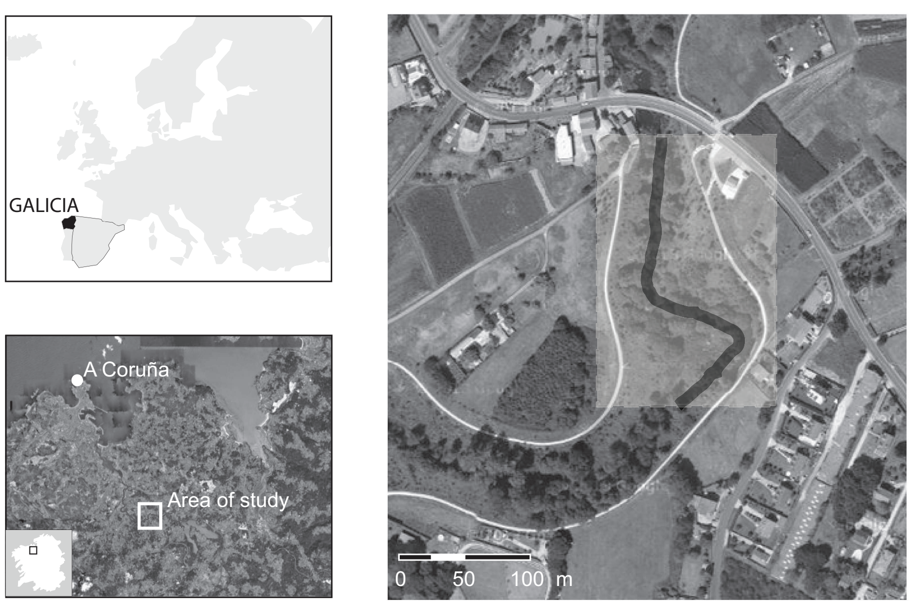

Figure 3



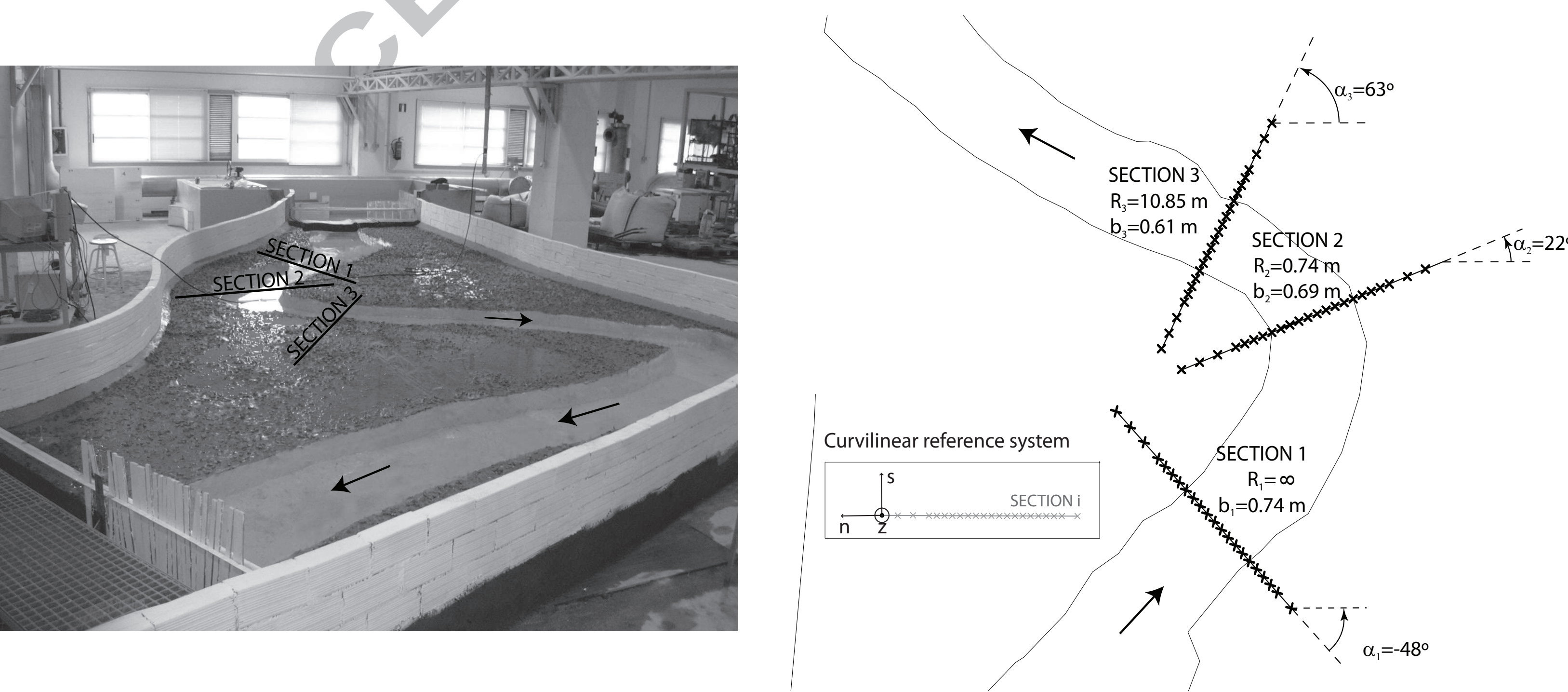
SECTION 1
SECTION 2
SECTION 3
SECTION 3
$R_3$=10.85 m
$b_3$=0.61 m
SECTION 2
$R_2$=0.74 m
$b_2$=0.69 m
SECTION 1
$R_1=\infty$
$b_1$=0.74 m
$\alpha_3$=63º
$\alpha_2$=22º
$\alpha_1$=-48º
Curvilinear reference system
s
n
z
SECTION i

Figure 4



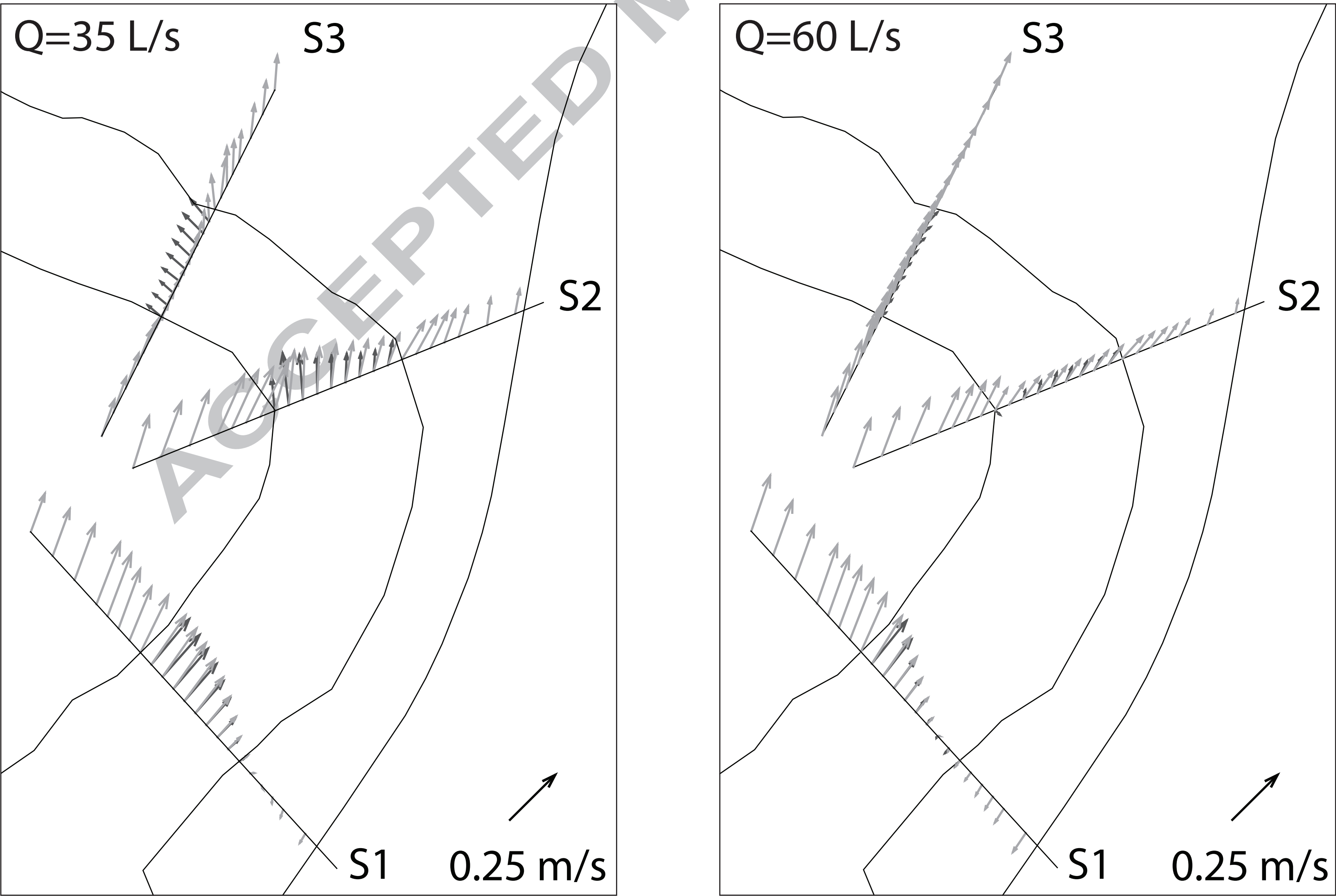

Figure 5



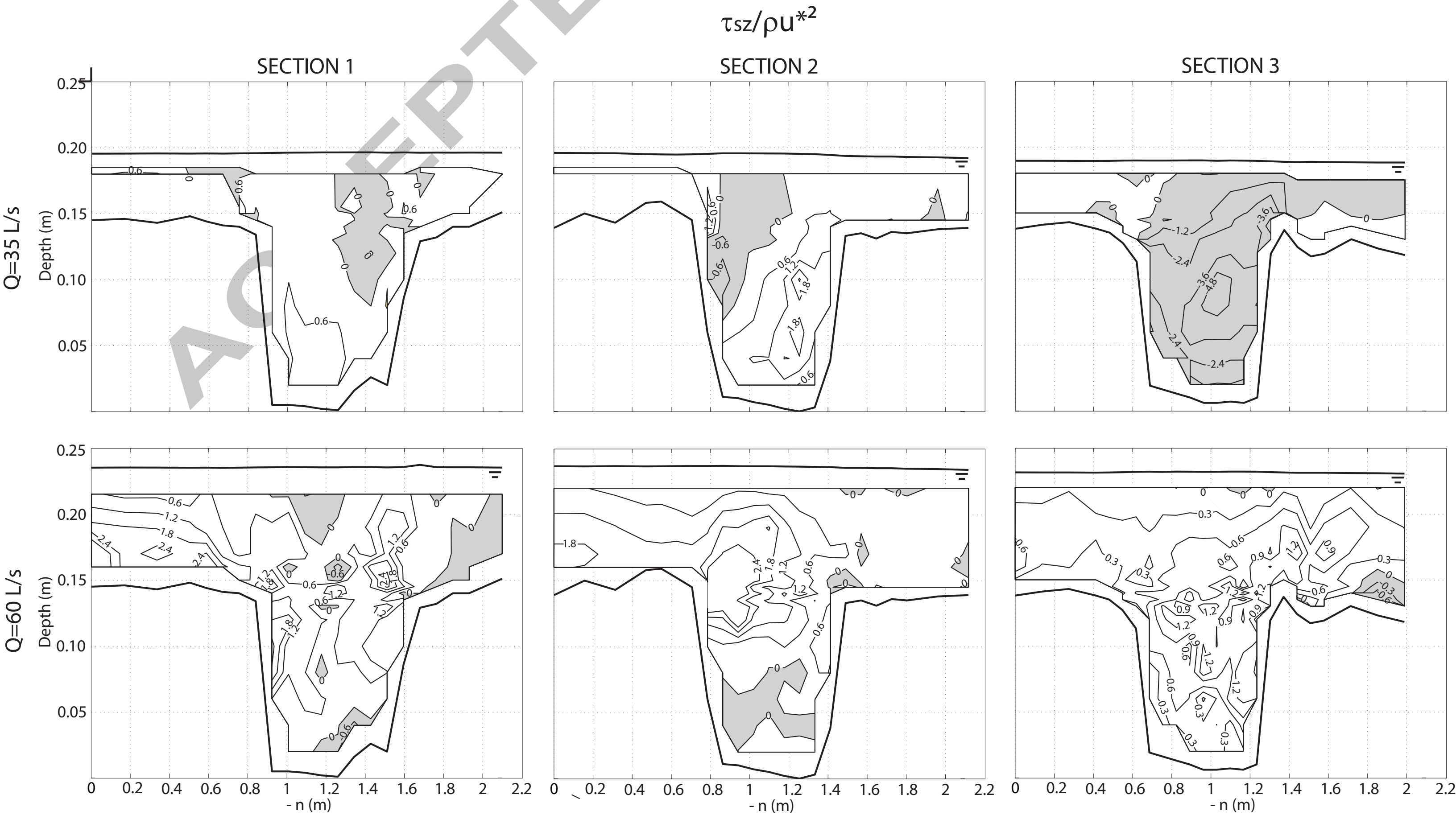
τsz/ρu*²
SECTION 1
SECTION 2
SECTION 3
Q=35 L/s
Q=60 L/s
Depth (m)
- n (m)
0.25
0.20
0.15
0.10
0.05
0 0.2 0.4 0.6 0.8 1 1.2 1.4 1.6 1.8 2 2.2

Figure 6



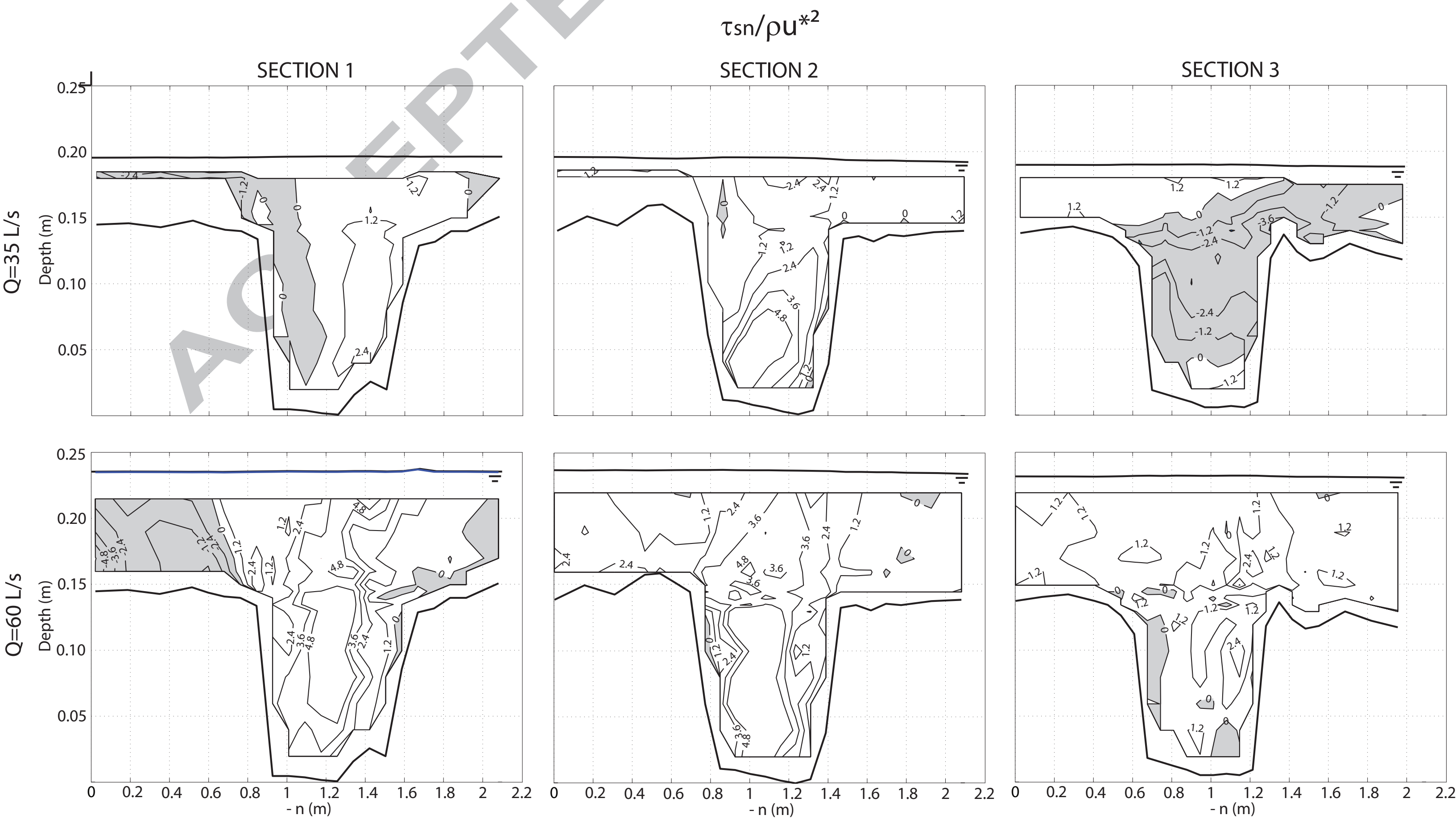

Figure 7



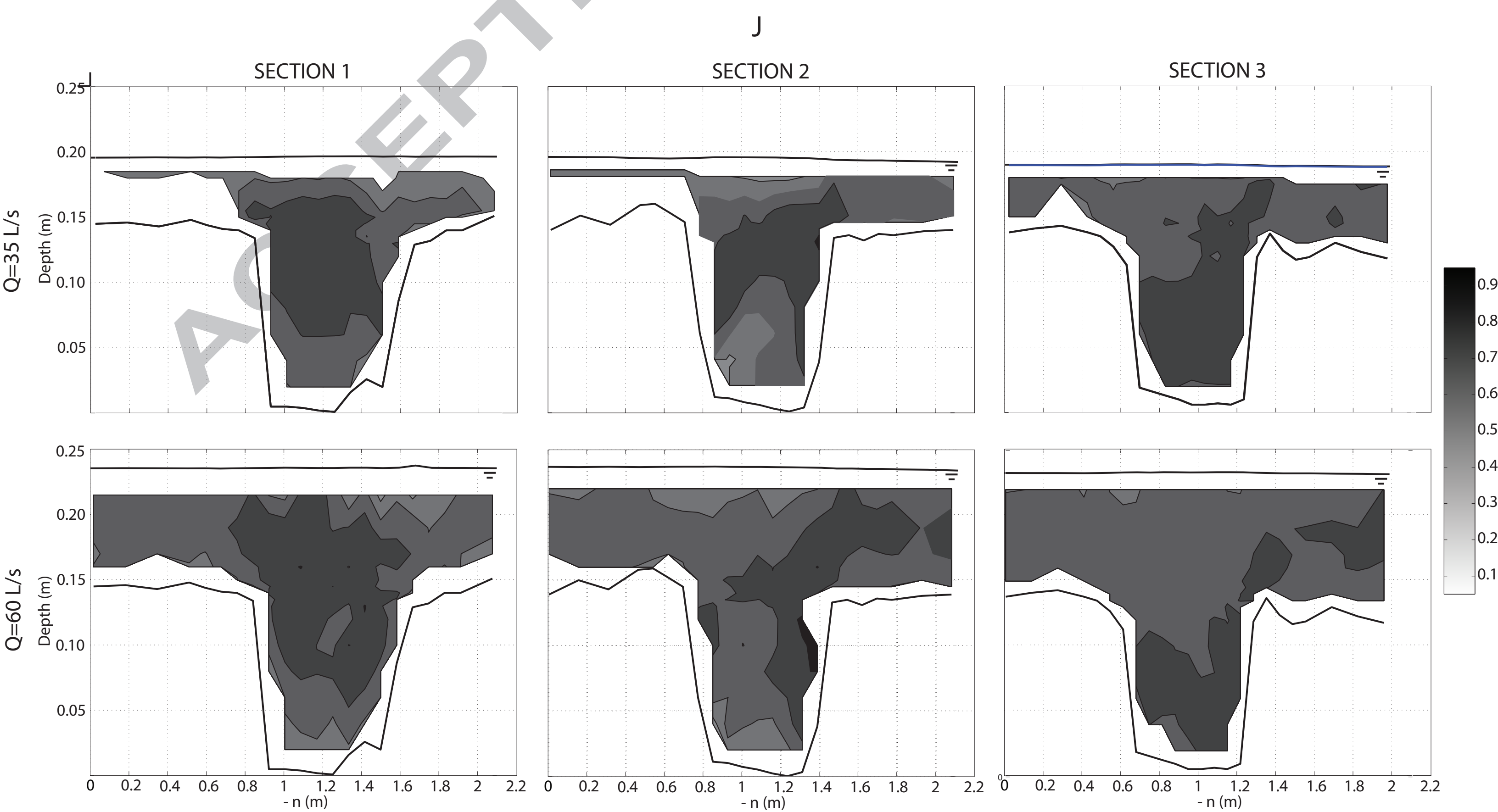
J
SECTION 1
SECTION 2
SECTION 3
Q=35 L/s
Q=60 L/s
Depth (m)
- n (m)
0.25
0.20
0.15
0.10
0.05
0 0.2 0.4 0.6 0.8 1 1.2 1.4 1.6 1.8 2 2.2
0.9
0.8
0.7
0.6
0.5
0.4
0.3
0.2
0.1

Figure 8



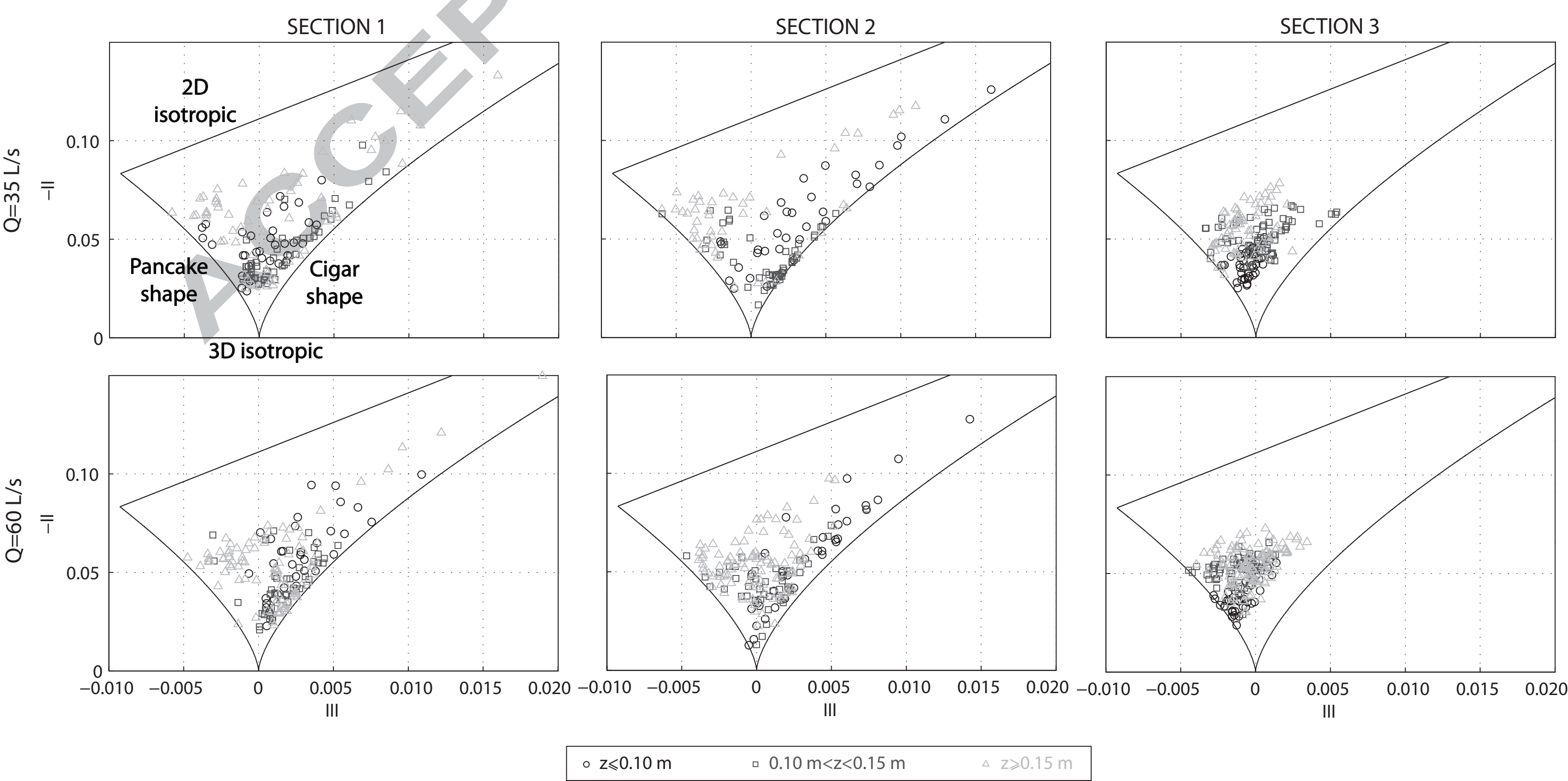
SECTION 1
SECTION 2
SECTION 3
2D isotropic
Pancake shape
Cigar shape
3D isotropic
Q=35 L/s
Q=60 L/s
−II
III
0
0.05
0.10
−0.010
−0.005
0.005
0.010
0.015
0.020
z⩽0.10 m
0.10 m<z<0.15 m
z⩾0.15 m

Figure 9



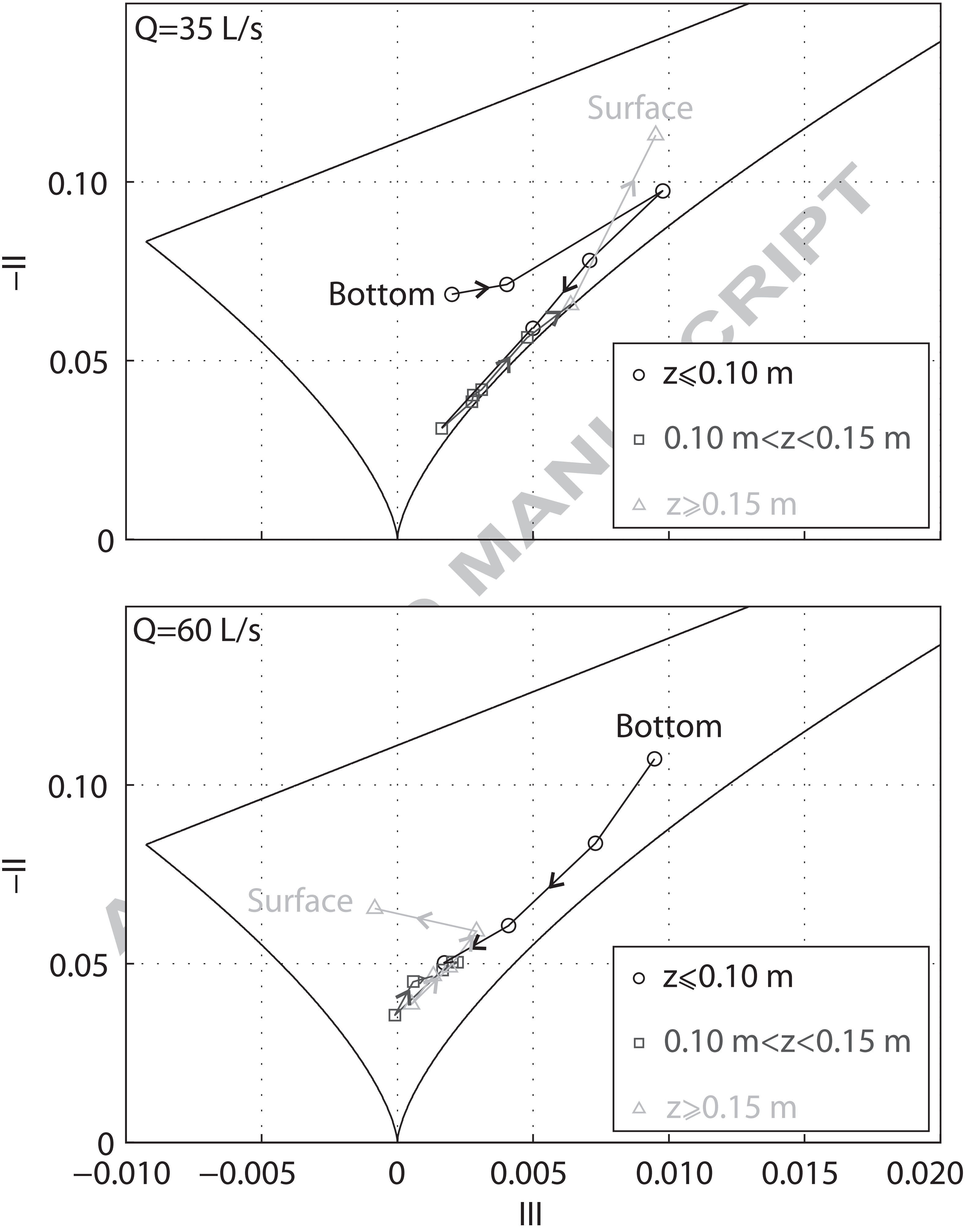

Q=35 L/s
Surface
Bottom
0.10
0.05
0
-II
z⩽0.10 m
0.10 m<z<0.15 m
z⩾0.15 m
Q=60 L/s
Bottom
Surface
0.10
0.05
0
-II
z⩽0.10 m
0.10 m<z<0.15 m
z⩾0.15 m
−0.010
−0.005
0
0.005
0.010
0.015
0.020
III

Figure 10



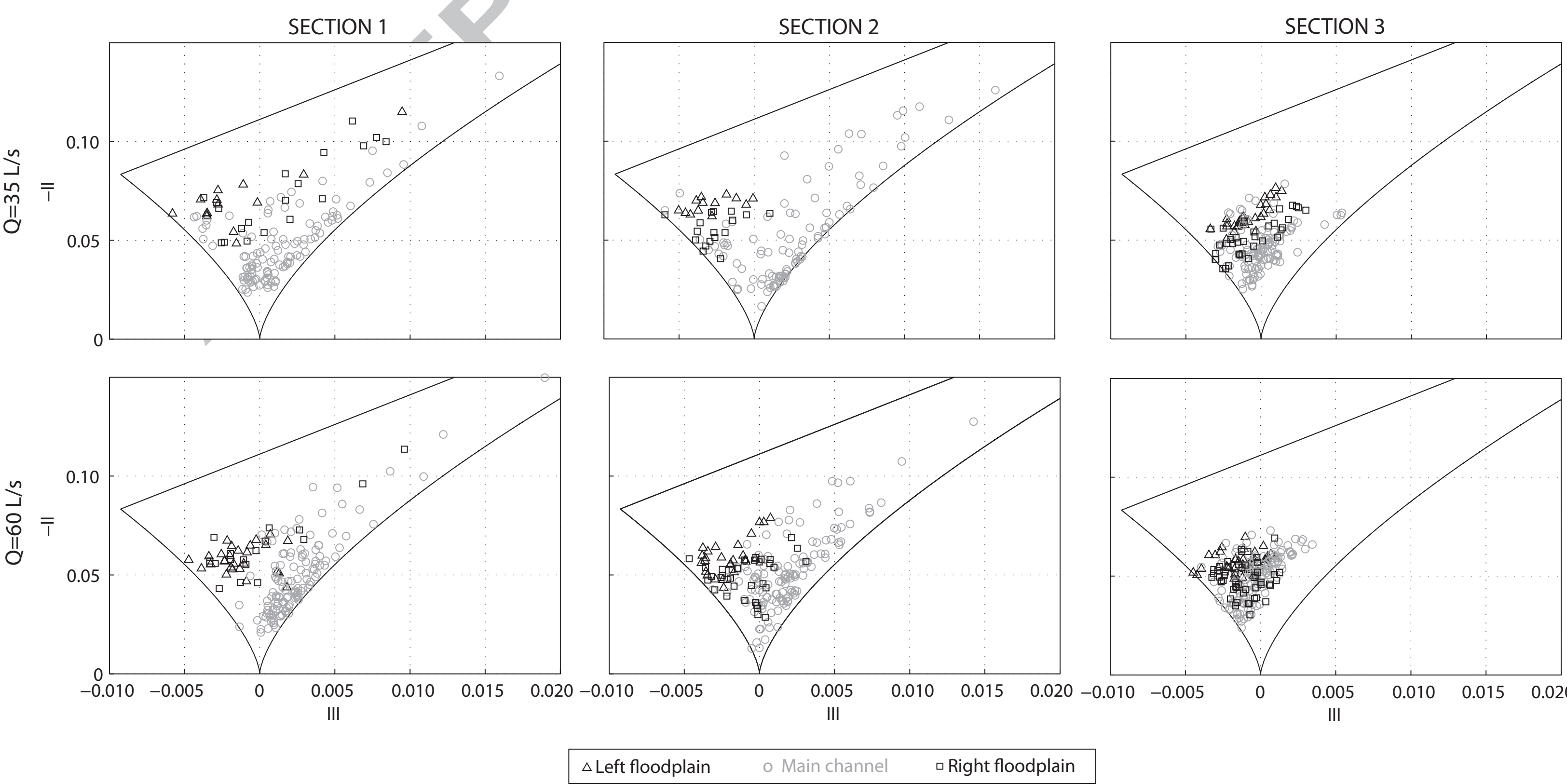
SECTION 1
SECTION 2
SECTION 3
Q=35 L/s
−II
Q=60 L/s
−II
0.10
0.05
0
−0.010
−0.005
0
0.005
0.010
0.015
0.020
III
△ Left floodplain
○ Main channel
□ Right floodplain

Figure 11



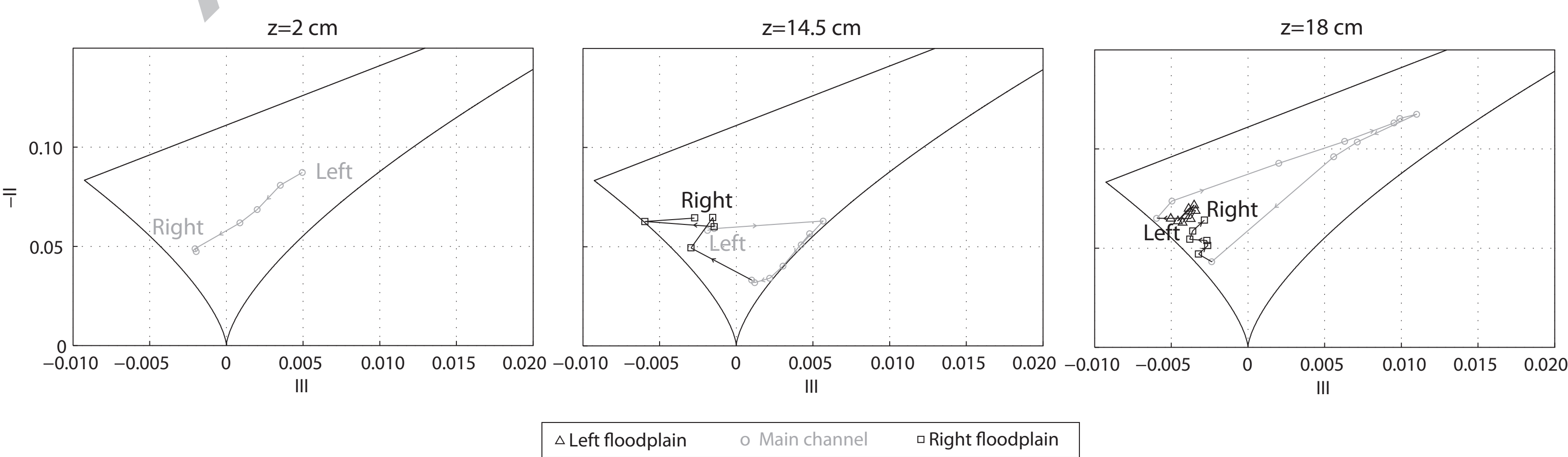
z=2 cm
z=14.5 cm
z=18 cm
−II
III
Left
Right
0.10
0.05
0
−0.010
−0.005
0.005
0.010
0.015
0.020
Left floodplain
Main channel
Right floodplain

Figure 12



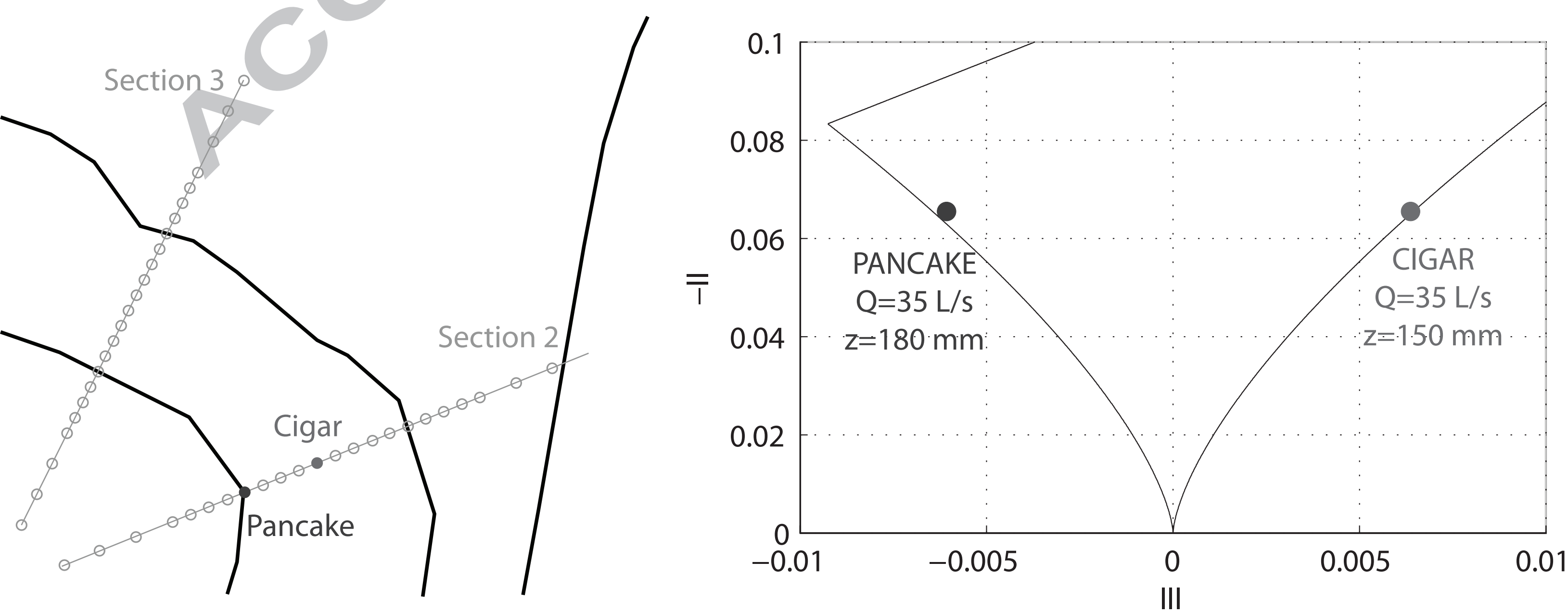
Section 3
Section 2
Cigar
Pancake
0.1
0.08
0.06
0.04
0.02
0
−0.01
−0.005
0
0.005
0.01
II
III
PANCAKE
Q=35 L/s
z=180 mm
CIGAR
Q=35 L/s
z=150 mm

Figure 13



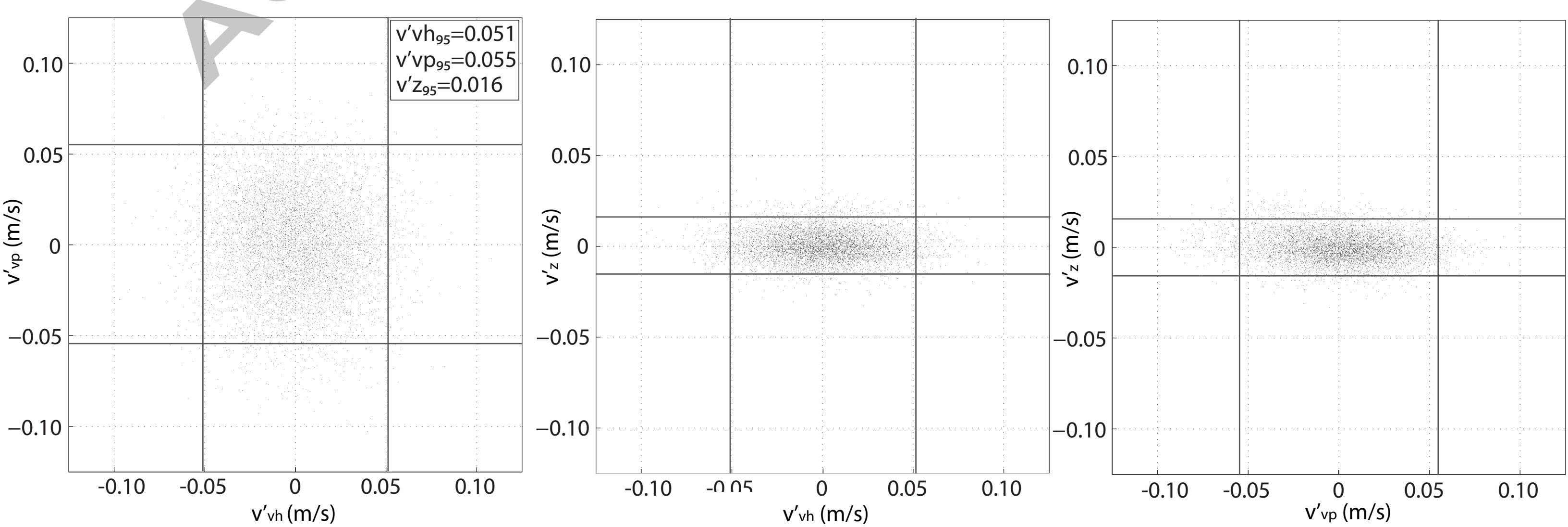
v′vh$_{95}$=0.051
v′vp$_{95}$=0.055
v′z$_{95}$=0.016
v′$_{vp}$ (m/s)
v′$_{vh}$ (m/s)
v′$_{z}$ (m/s)
v′$_{vh}$ (m/s)
v′$_{z}$ (m/s)
v′$_{vp}$ (m/s)
0.10
0.05
0
−0.05
−0.10
-0.10
-0.05
0
0.05
0.10

Figure 14



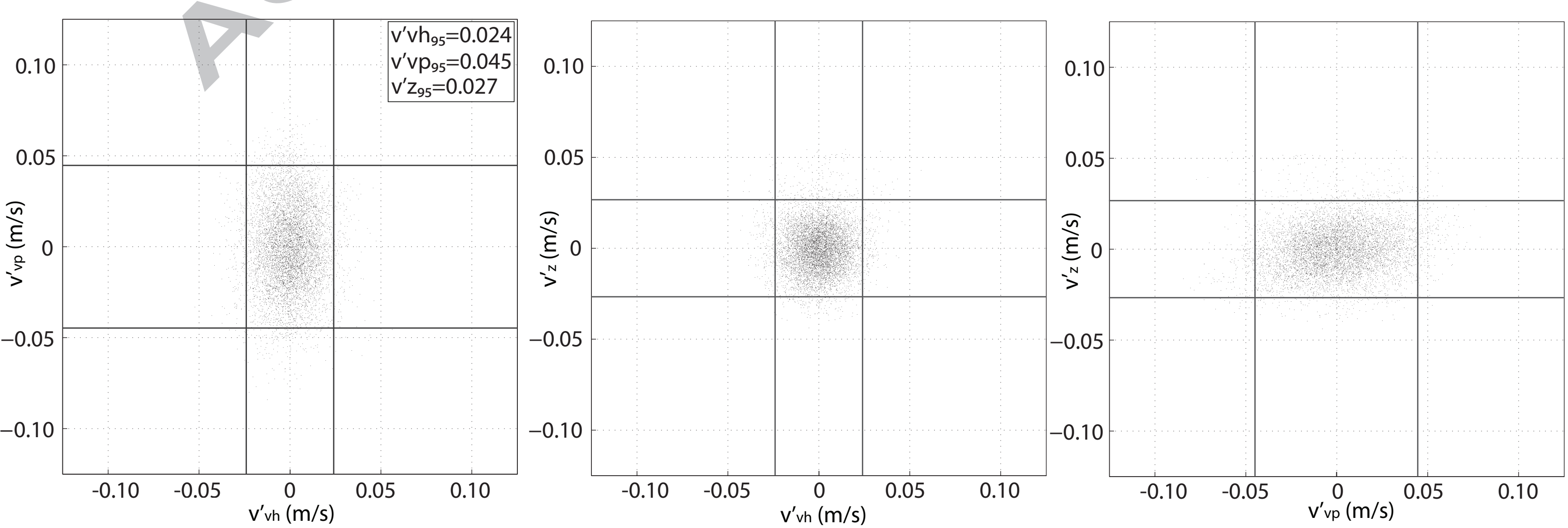
v′vh95=0.024
v′vp95=0.045
v′z95=0.027
v′vp (m/s)
v′vh (m/s)
v′z (m/s)
v′vh (m/s)
v′z (m/s)
v′vp (m/s)
0.10
0.05
0
−0.05
−0.10
-0.10
-0.05
0
0.05
0.10

# Turbulence anisotropy in a compound meandering channel with different submergence conditions

Mera, I. [a]; Franca, M. J. [b]; Anta, J. [a]; Peña, E. [a]

[a] *Water and Environmental Engineering Group- University of A Coruña. ETSI Caminos, Canales y Puertos. Campus de Elviña s/n, 15071 A Coruña, SPAIN. Emails:* imera@udc.es, jose.anta@udc.es, epena@udc.es

[b] *Laboratoire de Constructions Hydrauliques (LCH) - École Polytechnique Fédérale de Lausanne. Station 18, LCH-ENAC-EPFL CH-1015 Lausanne, SWITZERLAND. Email:* mario.franca@epfl.ch

**HIGHLIGHTS**

**- The hydrodynamics of a real compound meander are analyzed in a physical model**

**- Tridimensional velocities and mass transfer are characterized**

**- Turbulence is analyzed with a technique irrespective of the referential of measurements**

**- Turbulent structures are identified and related to mean flow features**

# Turbulence anisotropy in a compound meandering channel with different submergence conditions

Mera, I. [a]; Franca, M. J. [b]; Anta, J. [a]; Peña, E. [a]

[a] *Water and Environmental Engineering Group- University of A Coruña. ETSI Caminos, Canales y Puertos. Campus de Elviña s/n, 15071 A Coruña, SPAIN. Emails: imera@udc.es, jose.anta@udc.es, epena@udc.es*

[b] *Laboratoire de Constructions Hydrauliques (LCH) - École Polytechnique Fédérale de Lausanne. Station 18, LCH-ENAC-EPFL CH-1015 Lausanne, SWITZERLAND. Email: mario.franca@epfl.ch*

## GRAPHICAL ABSTRACT

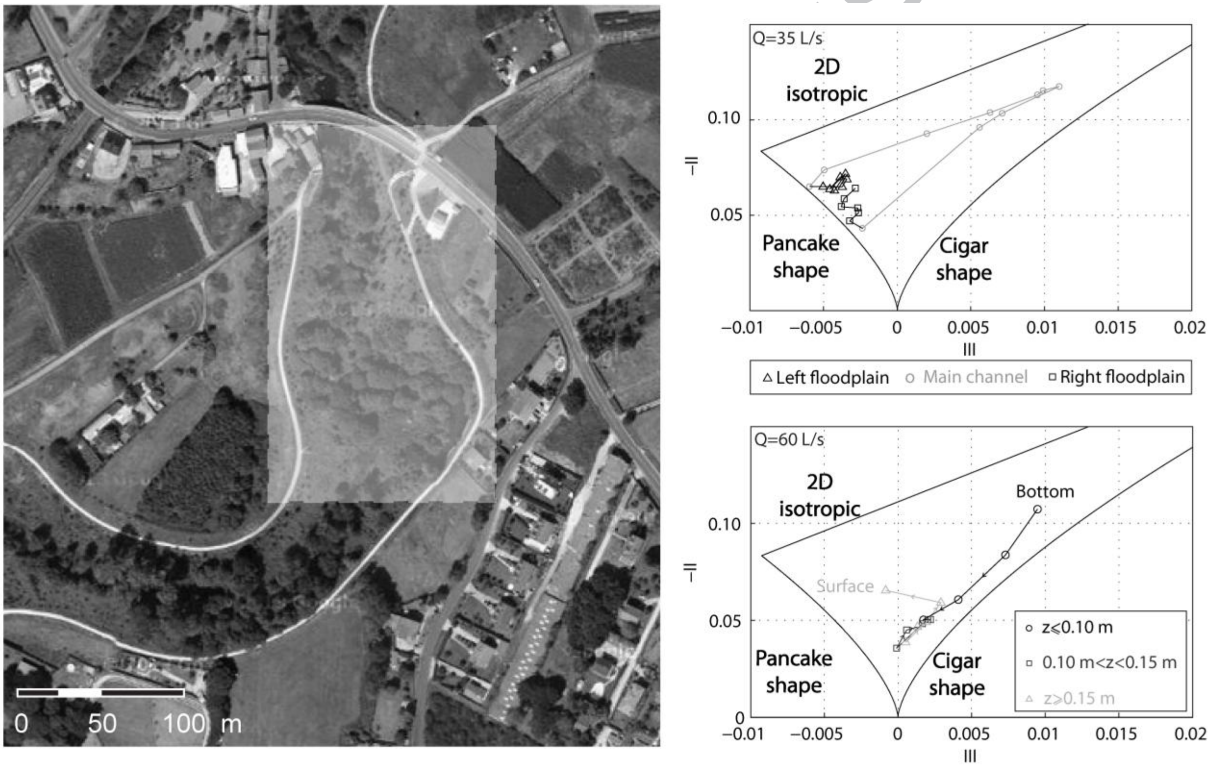


Aerial photograph of the river reach with a compound meander modelled in the laboratory and distribution of the anisotropy invariants across the section and throughout the water column for two different submergence conditions (*Q*=35 and *Q*=60 L/s)